RESEARCH ARTICLE

Figures and figure supplements

Cell-cell interaction determines cell fate of mesoderm-derived cell in tongue development through Hh signaling

Maiko Kawasaki *et al.*

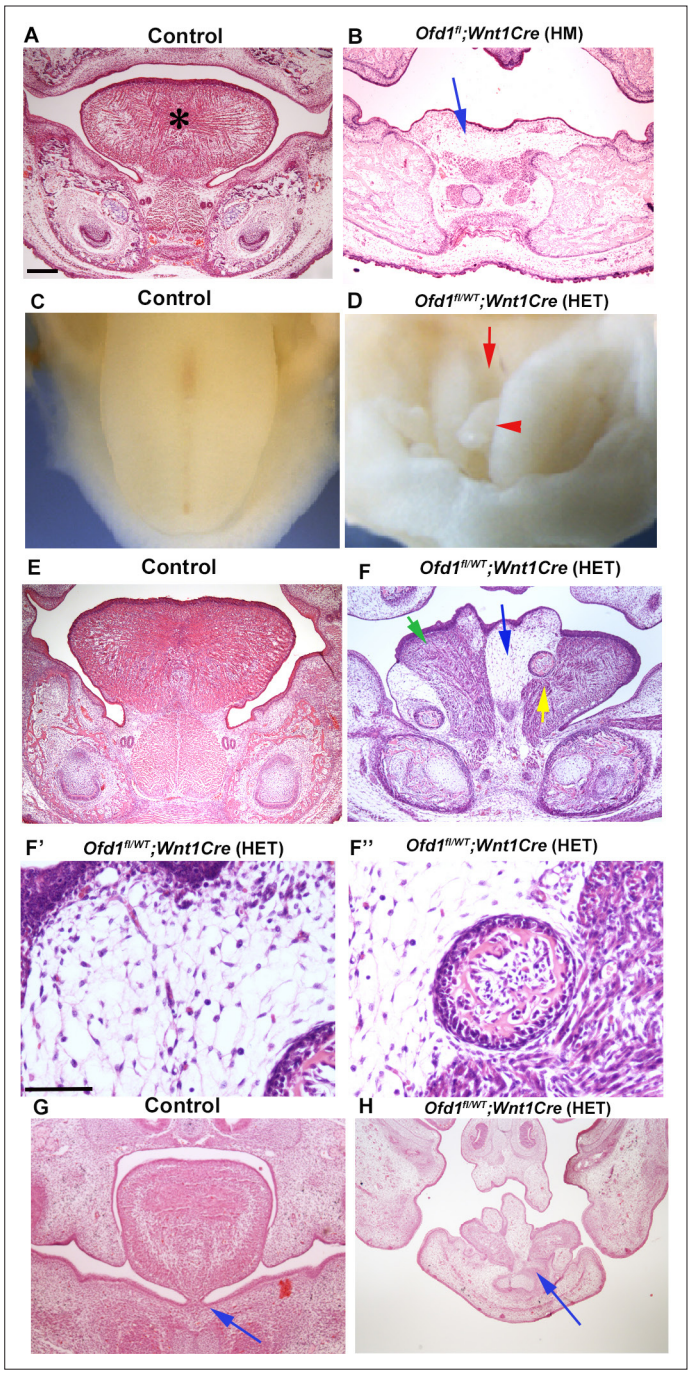

Figure 1. Tongue phenotypes in *Ofd1* mutant mice. (**A, B, E–H**) Frontal sections showing histological images in wild-type (**A, E, G**), *Ofd1*^{fl};*Wnt1Cre*(HM) (**B**) and *Ofd1*$^{fl/WT}$;*Wnt1Cre*(HET) (**F–F'', H**) at embryonic day (E) 18.5. Arrow indicating sparse tissue (**B**). *: tongue (**A**). Green, blue, and yellow arrows indicating normal muscle, ectopic sparse tissue, and ectopic bone, respectively (**F**). F′ and F″ are high magnification of F indicated by blue and yellow arrow, respectively. Arrows indicating tongue frenum region (**G, H**). The presence of clefts and multiple protrusions; n=58/58. (**C, D**) Image showing oral view of tongue in wild-type (**C**) and *Ofd1*$^{fl/WT}$;*Wnt1Cre*(HET) (**D**). Arrowhead and arrow indicating ectopic protrusion and cleft, respectively (**D**). Lack of tongue frenum in *Ofd1*$^{fl/WT}$;*Wnt1Cre*(HET); n=30/58. Scale bars: 200 μm (A, B, E, F, G, H), 100 μm (F', F'').

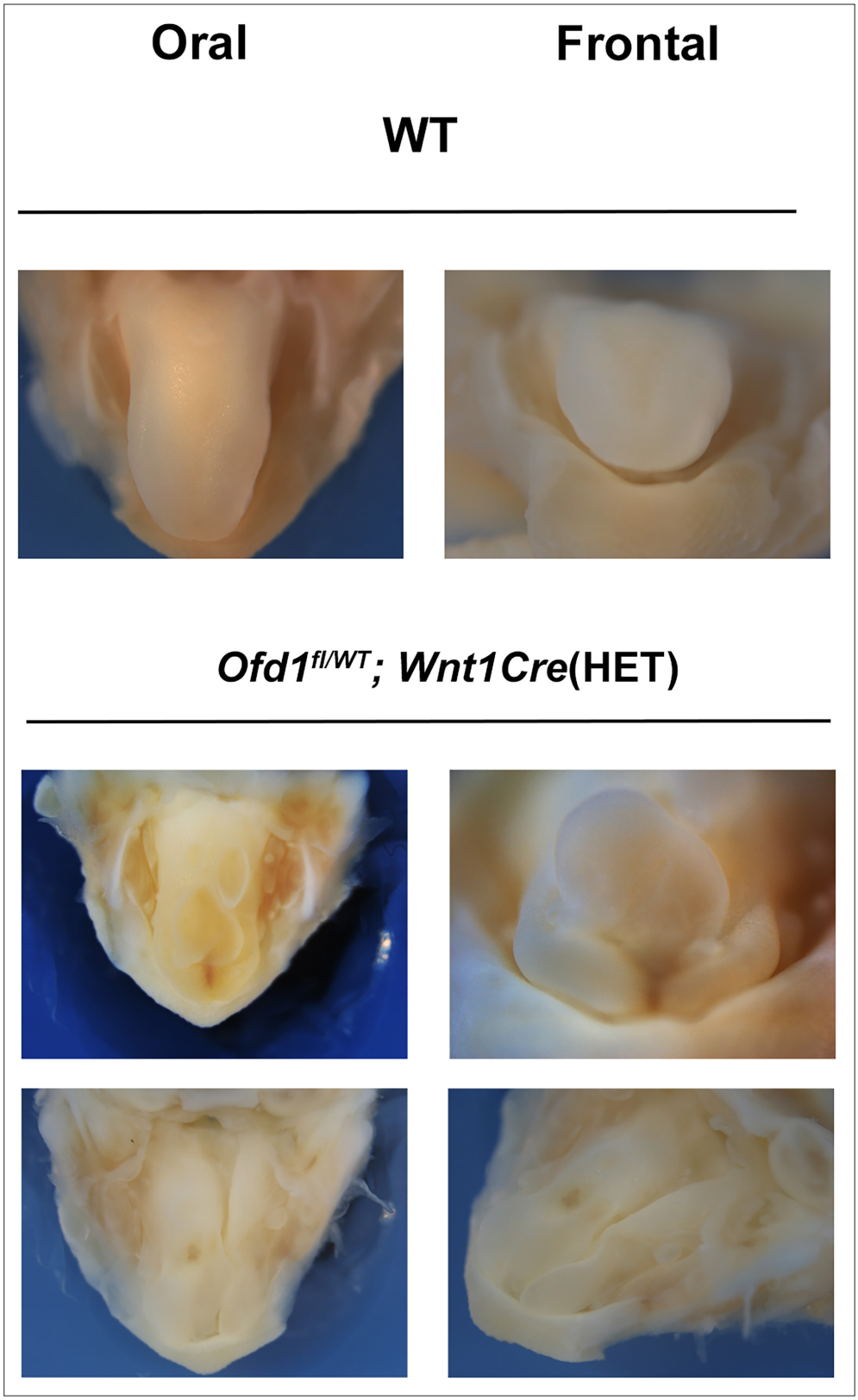

Figure 1—figure supplement 1. Abnormal shaped tongue in *Ofd1*$^{fl/WT}$;*Wnt1Cre*(HET) mice. Oral and frontal view of normal tongue in wild-type mice and abnormal shaped tongue in *Ofd1*$^{fl/WT}$;*Wnt1Cre*(HET) mice.

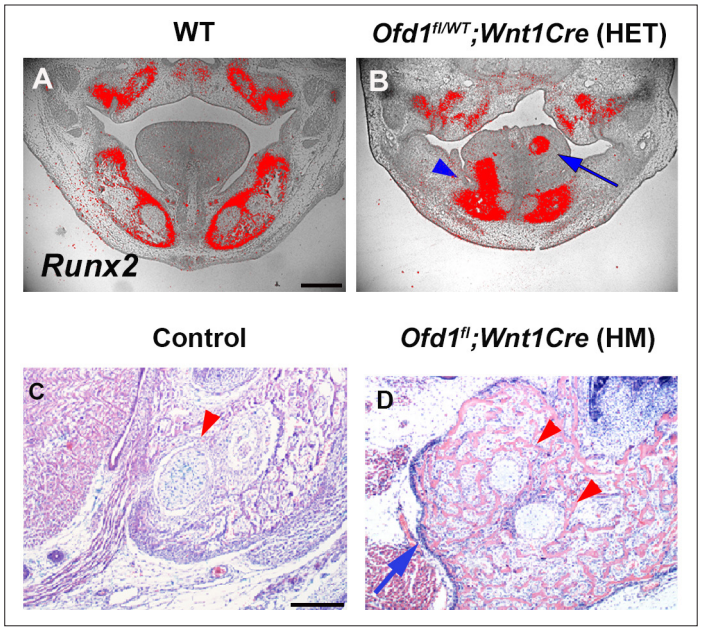

Figure 1—figure supplement 2. Bone in tongue of *Ofd1*$^{fl/WT}$;*Wnt1Cre*(HET) mice. Frontal sections showing in situ hybridization of *Runx2* (**A, B**) and histology (**C, D**) in wild-type (**A, C**) and *Ofd1*$^{fl/WT}$;*Wnt1Cre*(HET) (**B, D**). Arrow and arrowhead indicating bone region and connection between bone in the tongue and mandibular bone, respectively (**B**). Arrowheads and arrow indicating Meckel's cartilage and duplicated mandibular bone, respectively (**D**). Scale bars: 200 μm (A, B), 100 μm (C, D).

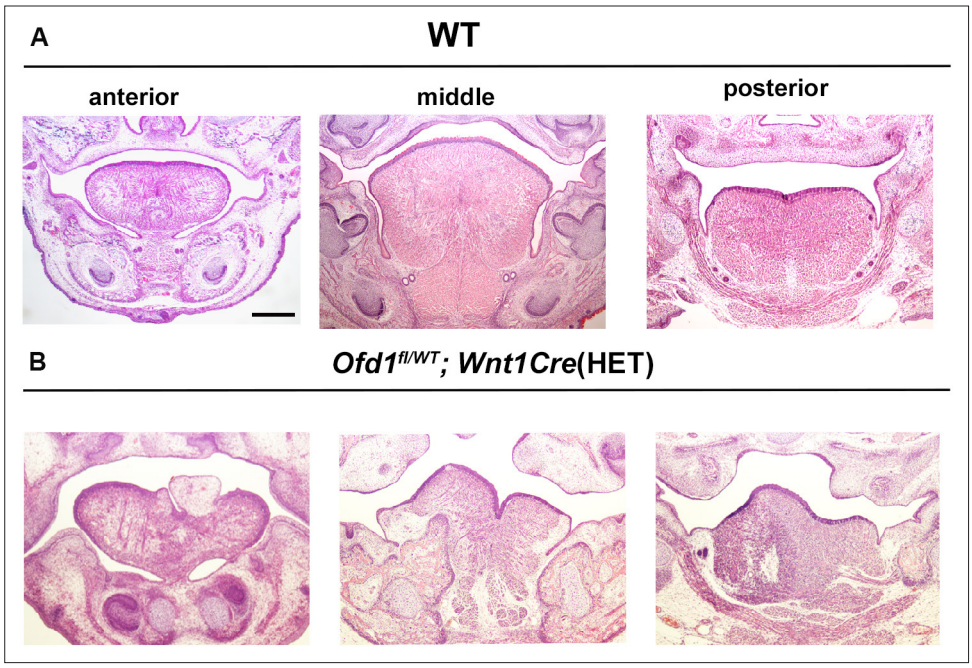

Figure 1—figure supplement 3. Tongue phenotypes in *Ofd1*$^{fl/WT}$;*Wnt1Cre*(HET) mice. Frontal section showing histological images of tongue in wild-type (**A**) and *Ofd1*$^{fl/WT}$;*Wnt1Cre*(HET) mice (**B**) at embryonic day (**E**) 18.5. Scale bars: 200 μm (**A, B**).

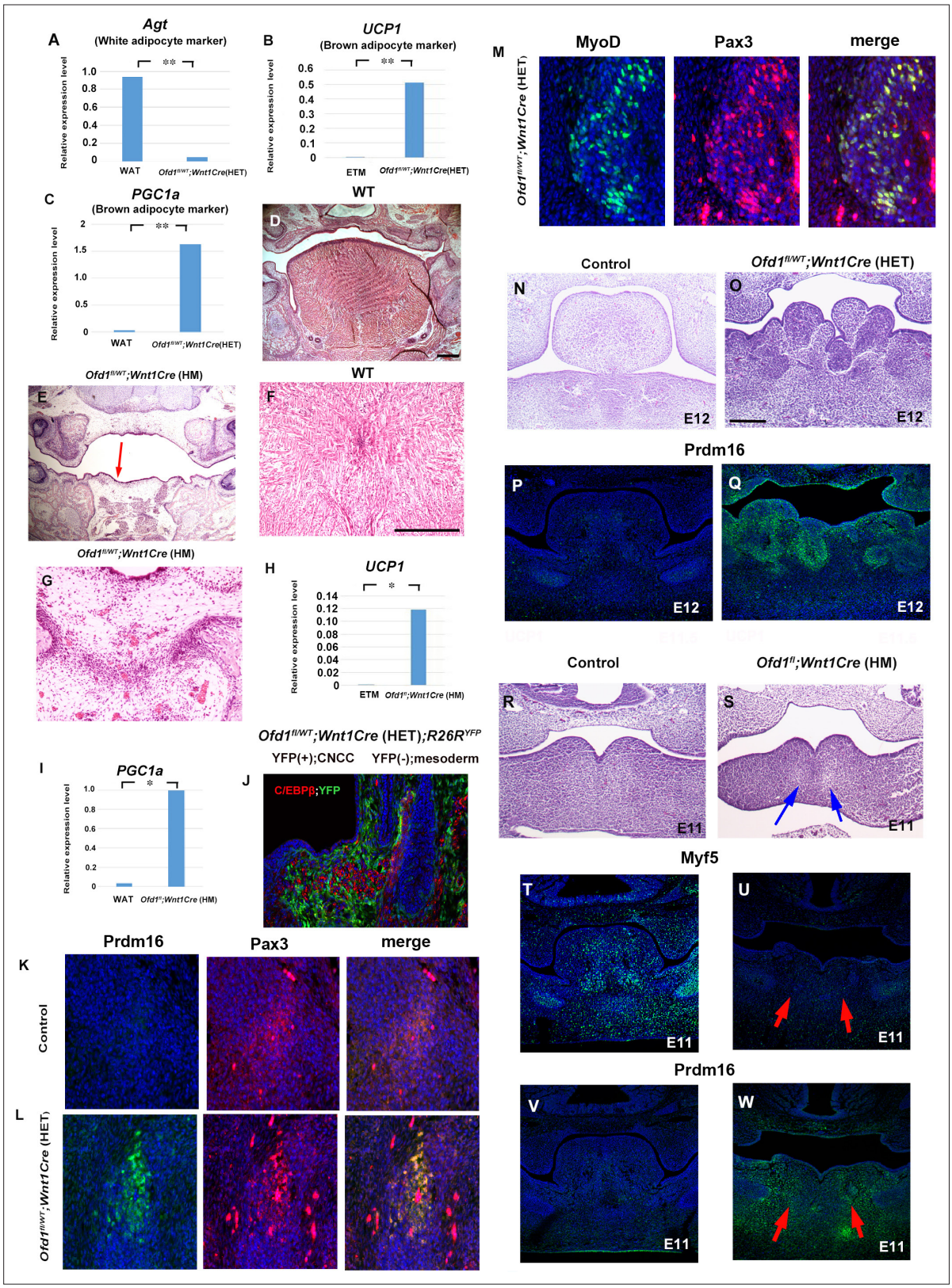

Figure 2. Sparse tissue in *Ofd1* mutant tongue. (**A–C**) Quantitative PCR (q-PCR) on mRNA isolated from ectopic sparse tissue, white adipose tissue (WAT), and embryonic tongue muscle (ETM). Expression of white adipose maker (*Agt*) was examined to understand whether the sparse tissue was white adipose maker. Only low-level expression of *Agt* in the sparse tissue compared with the WAT (**A**). Expression of brown adipose maker (*UCP1* and *PGC1a*) were examined to understand whether the sparse tissue was brown adipose maker. *UCP1* and *PGC1a* were expressed at high level in the

Figure 2 continued on next page

Figure 2 continued

sparse tissue, in comparison with those in the ETM (**B**) or adult WAT (**C**). **p<0.01. (**D–G**) Frontal sections showing histological images in wild-type (**D, F**) and *Ofd1*^{fl};*Wnt1Cre*(HM) (**E, G**). F and G are high magnification of D and E (indicated by blue arrow), respectively. (**H, I**) q-PCR on mRNA isolated from ectopic sparse tissue from *Ofd1*^{fl};*Wnt1Cre*(HM) mice, ETM and WAT. **p<0.01. (**J–M**) Frontal sections showing double immunohistochemistry of YFP and C/EBPβ in *Ofd1*$^{fl/WT}$;*Wnt1Cre*(HET);*R26R*^{YFP} (**D**), Prdm16 and Pax3 in wild-type (**K**) and *Ofd1*$^{fl/WT}$;*Wnt1Cre*(HET) (**L**), MyoD and Pax3 in *Ofd1*$^{fl/WT}$;*Wnt1Cre*(HET) (**M**) at embryonic day (E) 13.5. (**N–Q**) Frontal sections showing histological images (**N, O**) and immunohistochemistry of Prdm16 (**P, Q**) in wild-type (**N, P**) and *Ofd1*$^{fl/WT}$;*Wnt1Cre*(HET) mice at E12. (**R–W**) Frontal sections showing histological images (**R, S**) and immunohistochemistry of MyoD (**T, U**) and Prdm16 (**V, W**) in wild-type (**R, T, V**) and *Ofd1*^{fl};*Wnt1Cre*(HM) (**S, U, W**) mice at E11. Arrows indicating region showing sparse-like tissues. Scale bars: 200 μm (D, E, N, O, R, S), 100 μm (F, G).

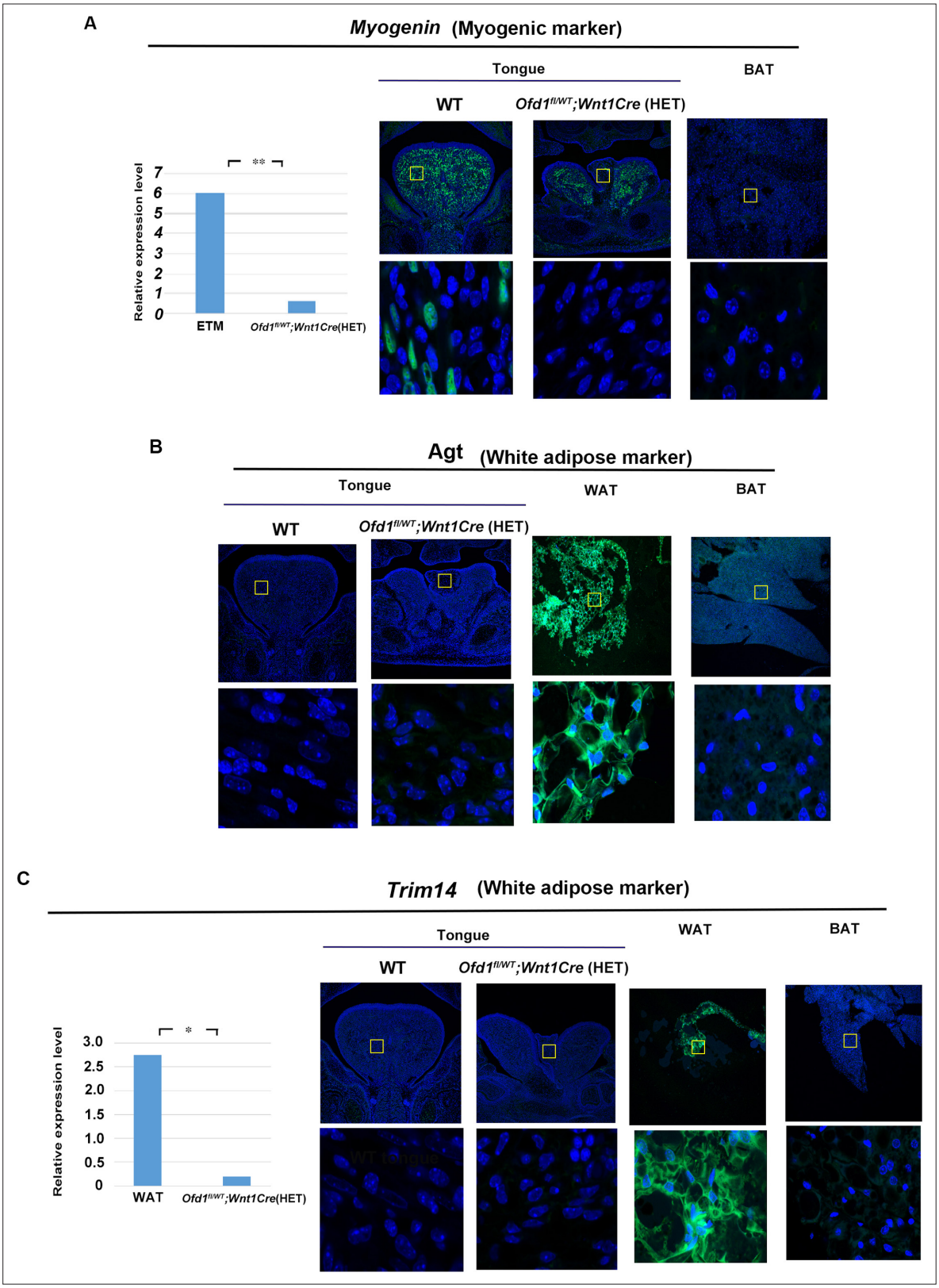

Figure 2—figure supplement 1. Quantitative PCR (q-PCR) and immunohistochemistry analysis (muscle and white adipose) on *Ofd1*$^{fl/WT}$;*Wnt1Cre*(HET) mice. (**A**) Myogenin (myogenic marker) was used to examine whether the sparse tissue was muscle. q-PCR of Myogenin on mRNA isolated from ectopic sparse tissue from *Ofd1*$^{fl/WT}$;*Wnt1Cre*(HET) and embryonic tongue muscle (ETM), and frontal sections showing immunohistochemistry of Myogenin in tongue of wild-type and *Ofd1*$^{fl/WT}$;*Wnt1Cre*(HET) mice, and matured brown adipose tissue (BAT; perirenal fat). Only low-level expression of Myogenin

Figure 2—figure supplement 1 continued on next page

Figure 2—figure supplement 1 continued

in the sparse tissue compared with the ETM. **p<0.01. Myogenin-positive cells could not be detected in the sparse tissue. (**B**) Agt (white adipose marker) was used to examine whether the sparse tissue was white adipose tissue (WAT). Frontal sections showing immunohistochemistry of Agt in tongue of wild-type and *Ofd1*$^{fl/WT}$;*Wnt1Cre*(HET) mice, WAT and BAT. Agt-positive cells could not be observed in the sparse tissue. (**C**) Trim14 (white adipose marker) was used to confirm that the sparse tissue was not WAT. q-PCR of Trim14 on mRNA isolated from ectopic sparse tissue from *Ofd1*$^{fl/WT}$;*Wnt1Cre*(HET) and WAT, and frontal sections showing immunohistochemistry of Trim14 in tongue of wild-type and *Ofd1*$^{fl/WT}$;*Wnt1Cre*(HET) mice, BAT and WAT. Only low-level expression of Trim14 in the sparse tissue compared with the WAT. *p<0.05. Trim14-positive cells could not be observed in the sparse tissue. Lower panels in immunohistochemistry data; high magnification of regions outlined by boxes in upper panels.

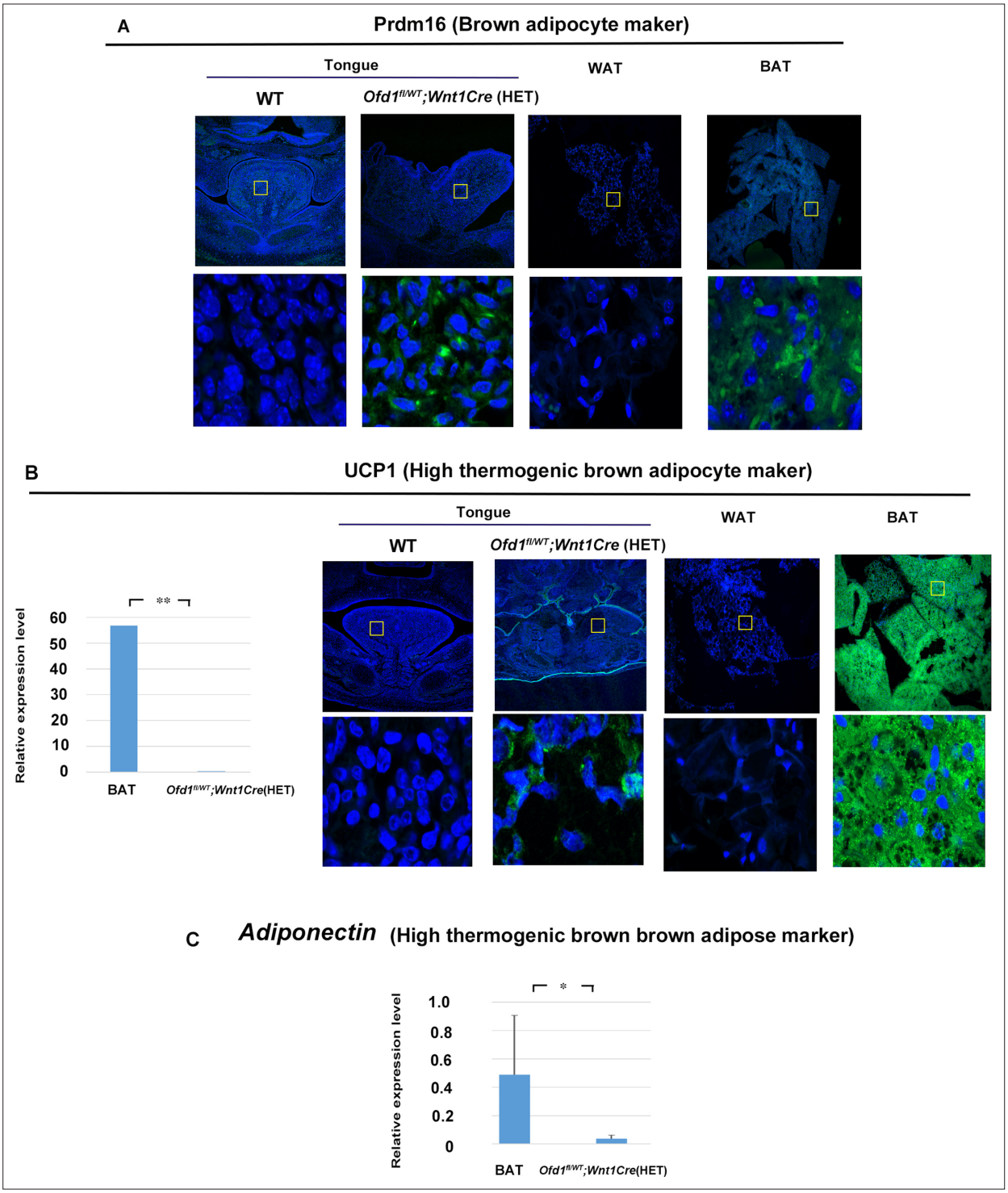

Figure 2—figure supplement 2. Quantitative PCR (q-PCR) and immunohistochemistry analysis (brown adipose) on *Ofd1*$^{fl/WT}$;*Wnt1Cre*(HET) mice. (**A**) Prdm16 (brown adipose marker) was used to examine whether the sparse tissue was brown adipose tissue. Frontal sections showing immunohistochemistry of Prdm16 in tongue of wild-type and *Ofd1*$^{fl/WT}$;*Wnt1Cre*(HET) mice, BAT and WAT. Prdm16-positive cells could not be observed in the sparse tissue. (**B**) UCP1 (high thermogenic brown adipocyte marker) was used to examine whether the sparse tissue was brown adipose tissue consisting of high thermogenic brown adipocytes. q-PCR of UCP1 on mRNA isolated from ectopic sparse tissue from *Ofd1*$^{fl/WT}$;*Wnt1Cre*(HET) and BAT, and frontal sections showing immunohistochemistry of UCP1 in tongue of wild-type and *Ofd1*$^{fl/WT}$;*Wnt1Cre*(HET) mice, BAT and WAT. Only low-level expression of UCP1 in the sparse tissue compared with the BAT. **p<0.01. A few UCP1-positive cells could be detected in the sparse tissue. (**C**) Adiponectin (high thermogenic brown adipocyte marker) was used to examine whether the sparse tissue was brown adipose tissue consisting of high thermogenic brown adipocytes. q-PCR of Adiponectin on mRNA isolated from ectopic sparse tissue from *Ofd1*$^{fl/WT}$;*Wnt1Cre*(HET) and BAT. Only low-level expression of *UCP1* in the sparse tissue compared with the BAT. **p<0.01.

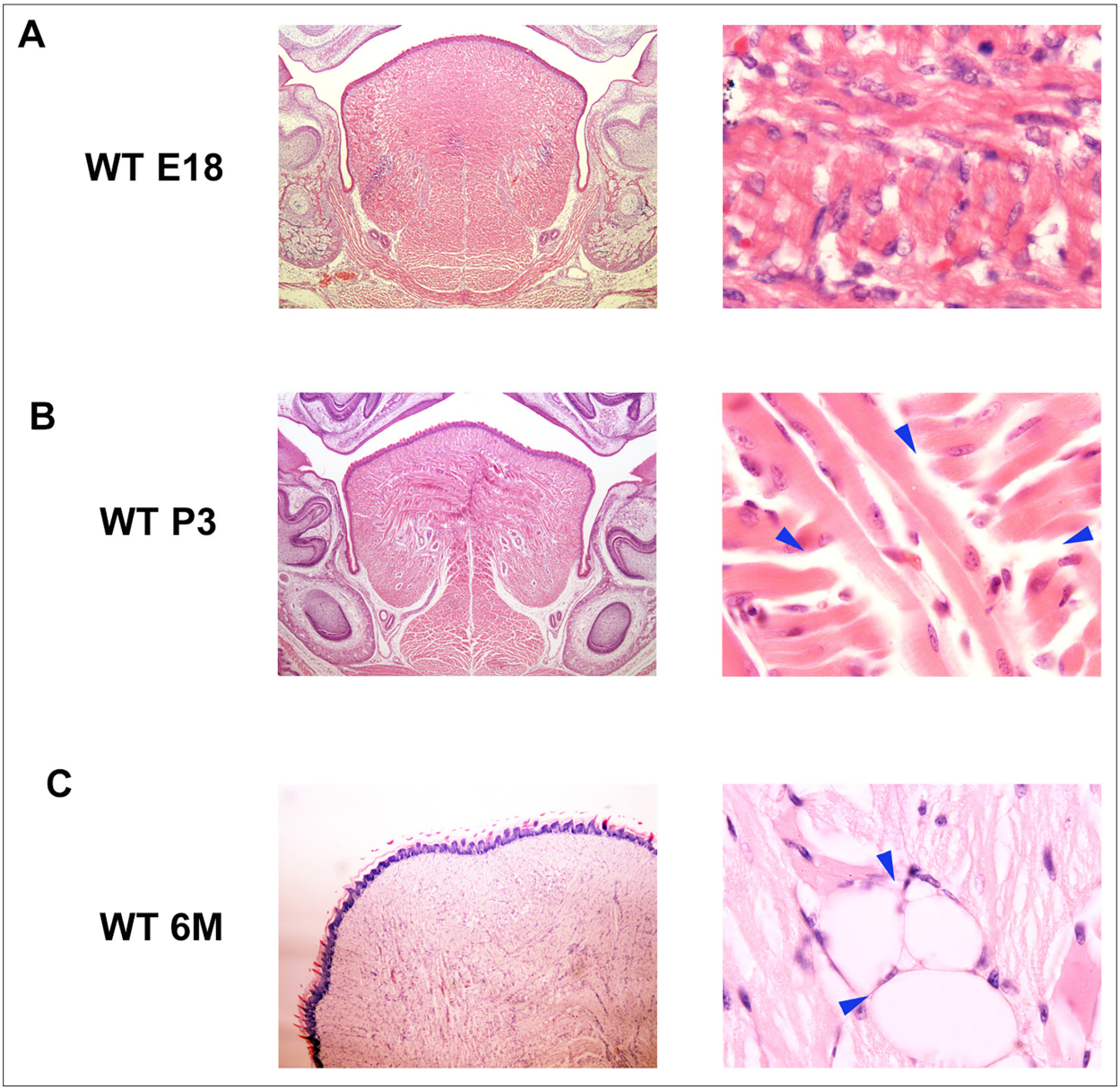

Figure 2—figure supplement 3. Artifact and adipose tissue in wild-type tongue. (**A, B**) Frontal sections showing empty spaces without surrounding cells in the tongue of prenatal (**A**) and postnatal (**B**) wild-type mice. Right panels are high magnification of left panels. Arrowheads indicating empty spaces. (**C**) Frontal sections showing intermuscular adipose in the tongue of 6-month-old wild-type mice. Arrowheads indicating adipocytes. P3, postnatal day 3; 6M, 6-month-old. Mucous salivary glands and their associated-adipose are known to be present in wild-type tongue. However, we could not identify any epithelial cells including glandular bodies or excretory ducts through immunohistochemistry around the sparse tissue. Adipose is also known to be present in the tongue as intermuscular adipose, which is often pathologically enlarged (***Colella et al., 2009***). However, it is known that the intermuscular adipose in the tongue is related to aging (***Vettor et al., 2009***; ***Scarda et al., 2010***). In prenatal or postnatal wild-type tongue, empty gaps were found between muscle bundles; however, adipocyte-like cells could not be observed around the gaps (**A, B**). However, empty gaps surrounded by cells with a thin rim of cytoplasm between muscle bundles were observed in older mice (**C**). Empty gaps between neighboring muscle fibers found in prenatal or postnatal wild-type tongue should be an artifact, as previously reported (***Rother et al., 2002***). Thus, the brown adipose tissue found in the *Ofd1* mutant tongue was not related to mucous salivary glands associated-adipose or intermuscular adipose.

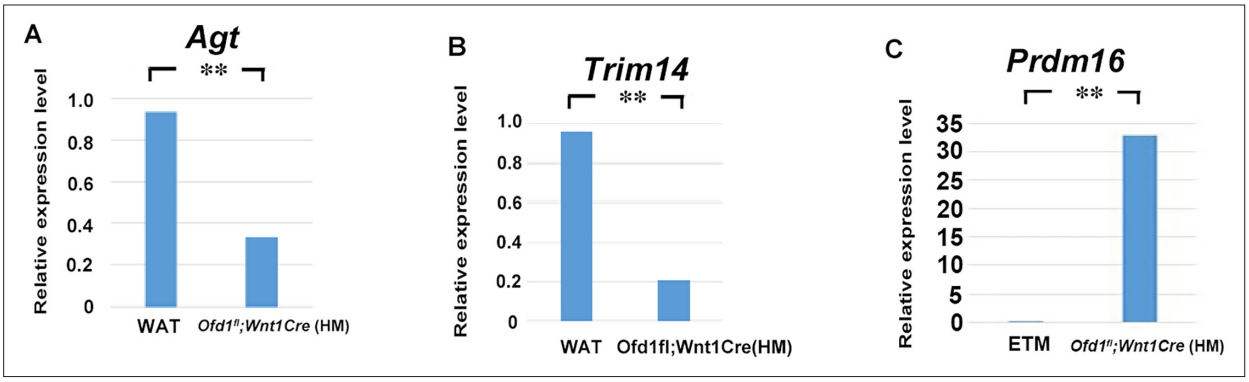

Figure 2—figure supplement 4. Quantitative PCR (q-PCR) analysis (adipose) on *Ofd1*^{fl};*Wnt1Cre*(HM) mice. q-PCR on mRNA isolated from ectopic sparse tissue of *Ofd1*^{fl};*Wnt1Cre*(HM), embryonic tongue muscle (ETM), and white adipose tissue (WAT). **p<0.01.

Figure 3. Interaction between cranial neural crest-derived cells (CNCC) and mesoderm-derived cells. (**A–D**) Frontal images of YFP expression (**A, B**) and *Myf5* expression of whole-mount in situ hybridization (**C, D**) in *Mesp1Cre;R26R*^{YFP} (**A**), *Wnt1Cre;R26R*^{YFP} (**B**), wild-type (**C**), and *Ofd1*^{fl}*;Wnt1Cre*(HM) (**D**) at embryonic day (E) 10. (**E, E'**) Frontal (**E**) and sagittal (**E**) view of LacZ stained *Osr2Cre;R26R*^{LacZ} mice at E10. (**F, G**) Frontal sections showing in situ hybridization of *Osr2* (**F**) and *MyoD* (**G**) in wild-type at E11. (**H**) Schematic diagram showing hypoglossal cord (left), CNCC (middle), and *Osr2-Cre*

Figure 3 continued on next page

Figure 3 continued

expression domain (right). (**I–L**) Frontal sections showing histological images in wild-type (**I**), *Ofd1*^{fl}*;Osr2Cre*(HM) (**L**), and *Ofd1*^{fl}*;Sox10Cre*(HM) (K, anterior and L, middle) at E16.5 (**K, L**) and E18.5 (**I, J**). (**M**) Double immunohistochemistry of YFP and MyoD on cultured YFP-expressing CNCC accompanied by YFP-negative mesoderm-derived cells obtained from *Wnt1Cre;R26R*^{YFP} mice. (**N**) Double immunohistochemistry of YFP and Prdm16 on cultured YFP-negative mesoderm-derived cells obtained from *Wnt1Cre;R26R*^{YFP} mice. (**Q**) Schematic diagram showing lateral view of craniofacial region with incision (red line). (**P, Q**) Double immunohistochemistry of MyoD and Prdm16 in cultured wild-type tongue without incision (**P**) and with incision (**Q**). Arrowheads indicating Prdm16-positive cells (**Q**).The presence of adipose tissue in explants with incisions, n=4/8; and without incision, n=0/8. Scale bars: 500μm (A-E'), 200 μm (I, J, K, L), 100 μm (F, G).

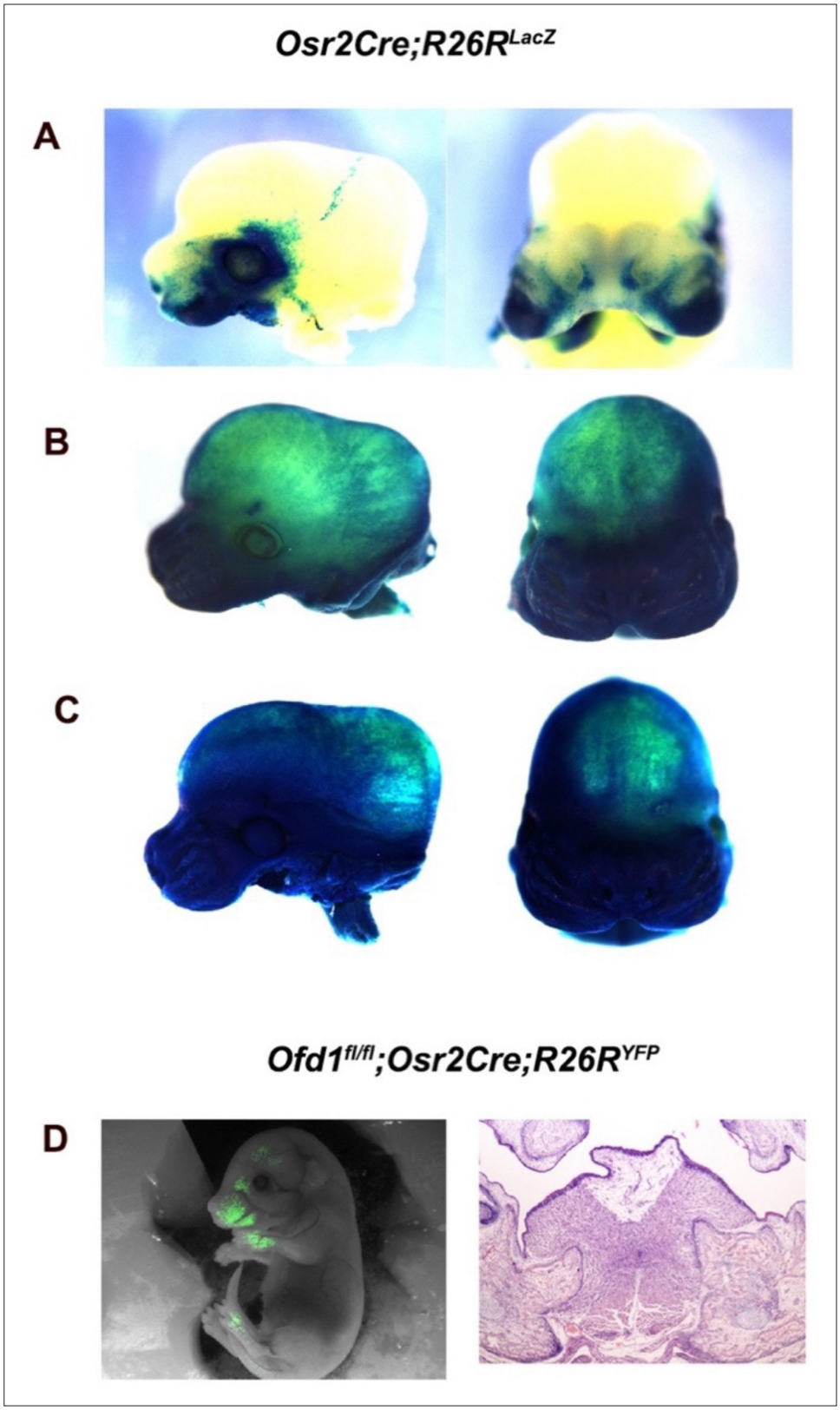

Figure 3—figure supplement 1. Variation of *Osr2-Cre* activation. *Osr2-Cre* activation (confirmed by LacZ staining in *Osr2Cre;R26R*^{LacZ}) exhibited the three different patterns (***Lan et al., 2007***). Most embryos displayed tissue-specific pattern consistent with specific Cre expression from the *Osr2* locus, as shown in A (tissue-specific pattern). Approximately 20% of *Osr2-Cre* displayed some ectopic activation, as shown in B (ectopic pattern). Approximately

Figure 3—figure supplement 1 continued on next page

Figure 3—figure supplement 1 continued

10% of *Osr2-Cre* embryos displayed almost ubiquitous activation, as shown in C (ubiquitous pattern). Abnormal tongue was observed in *Ofd1*^{fl}*;Osr2Cre;R26R*^{YFP} mice with tissue-specific pattern (**D**). *Ofd1*^{fl}*;Osr2Cre;R26R*^{YFP} mice with ectopic pattern or ubiquitous pattern led to early lethal, as previous paper reported (***Ferrante et al., 2006***). *Ofd1*^{fl}*;Osr2Cre;R26R*^{YFP} mice we can used in this study were tissue-specific pattern.

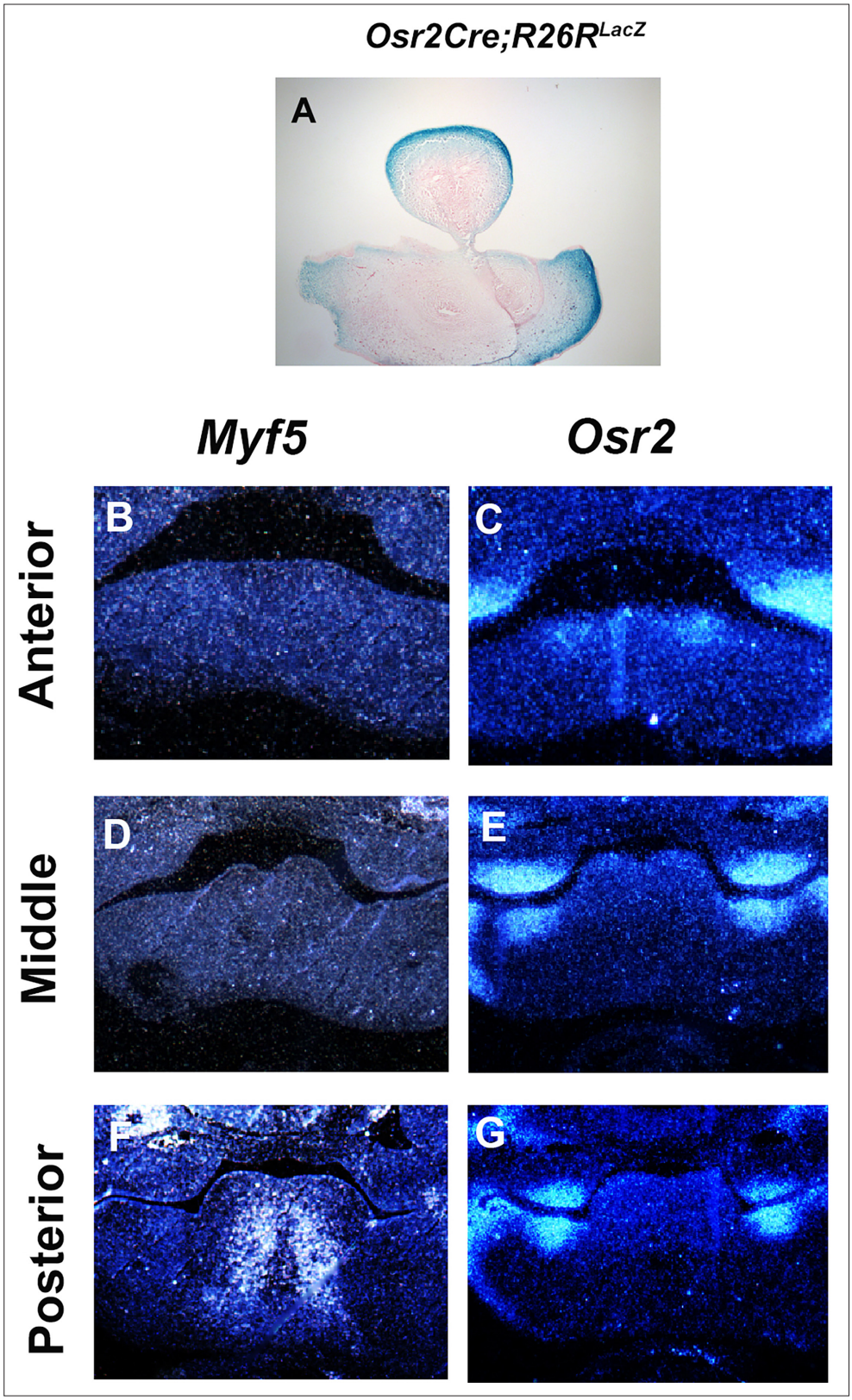

Figure 3—figure supplement 2. *Osr2* expression in developing tongue. (**A**) Frontal section showing LacZ stained *Osr2Cre;R26R*^{LacZ} mice at embryonic day (E) 13.5. (**B–G**) Frontal sections showing in situ hybridization of *Myf5* (**A–C**) and *Osr2* (**D–F**) in anterior (**A, D**), middle (**B, E**), and posterior (**C, F**) part of wild-type tongue at E11.5.

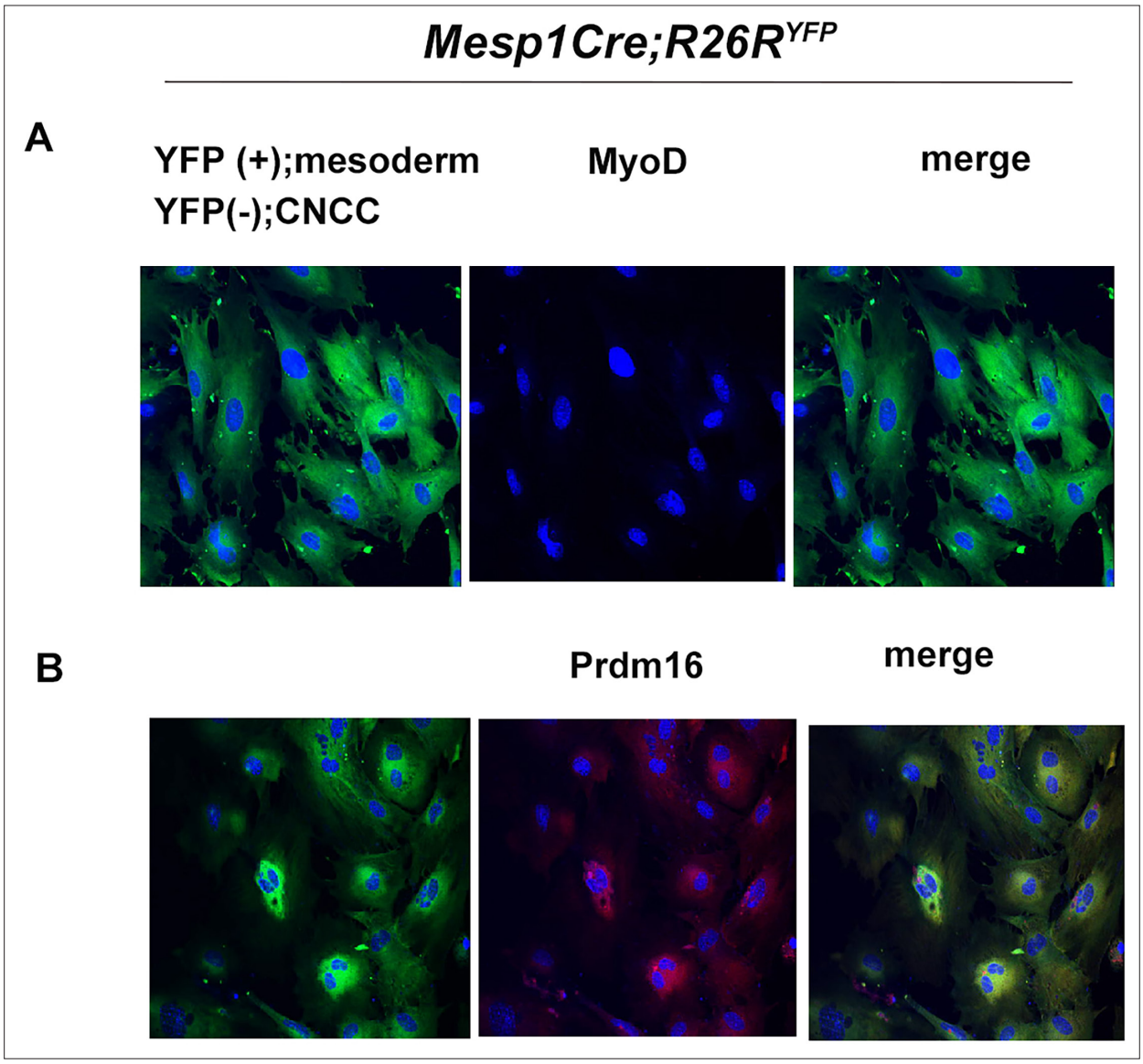

Figure 3—figure supplement 3. Interaction between cranial neural crest-derived cells (CNCC) and mesoderm-derived cells. Double immunohistochemistry of YFP and MyoD (**A**) and YFP and Prdm1 (**B**) on cultured YFP-expressing mesoderm-derived cells and YFP-negative CNCC obtained from *Mesp1Cre;R26R*^{YFP} mice.

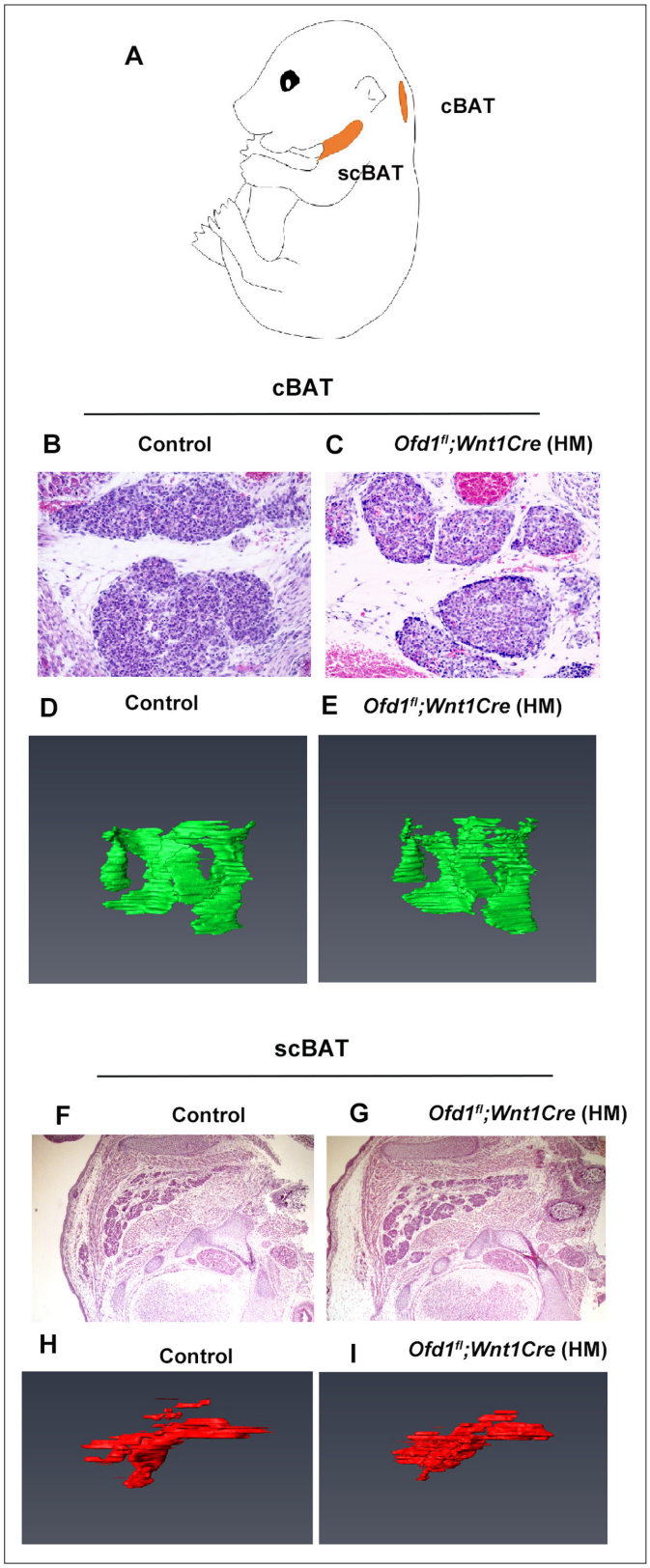

Figure 3—figure supplement 4. The cervical brown adipose tissue in *Ofd1*$^{fl/WT}$;*Wnt1Cre*(HET) mice. (**A**) Schematic diagram showing lateral view of supraclavicular (scBAT) and cervical (cBAT) brown adipose tissue. (**B, C, F, G**) Sagittal (**B, C**) and coronal (**F, G**) sections showing histology of scBAT and cBAT, respectively, in control (**B, F**) and *Ofd1*^{fl};*Wnt1Cre*(HM) (**C, G**) mice. (**D, E, H, I**) 3D reconstruction of scBAT and cBAT from serial sections of control (**D, H**) and *Ofd1*^{fl};*Wnt1Cre*(HM) (**E, I**) mice.

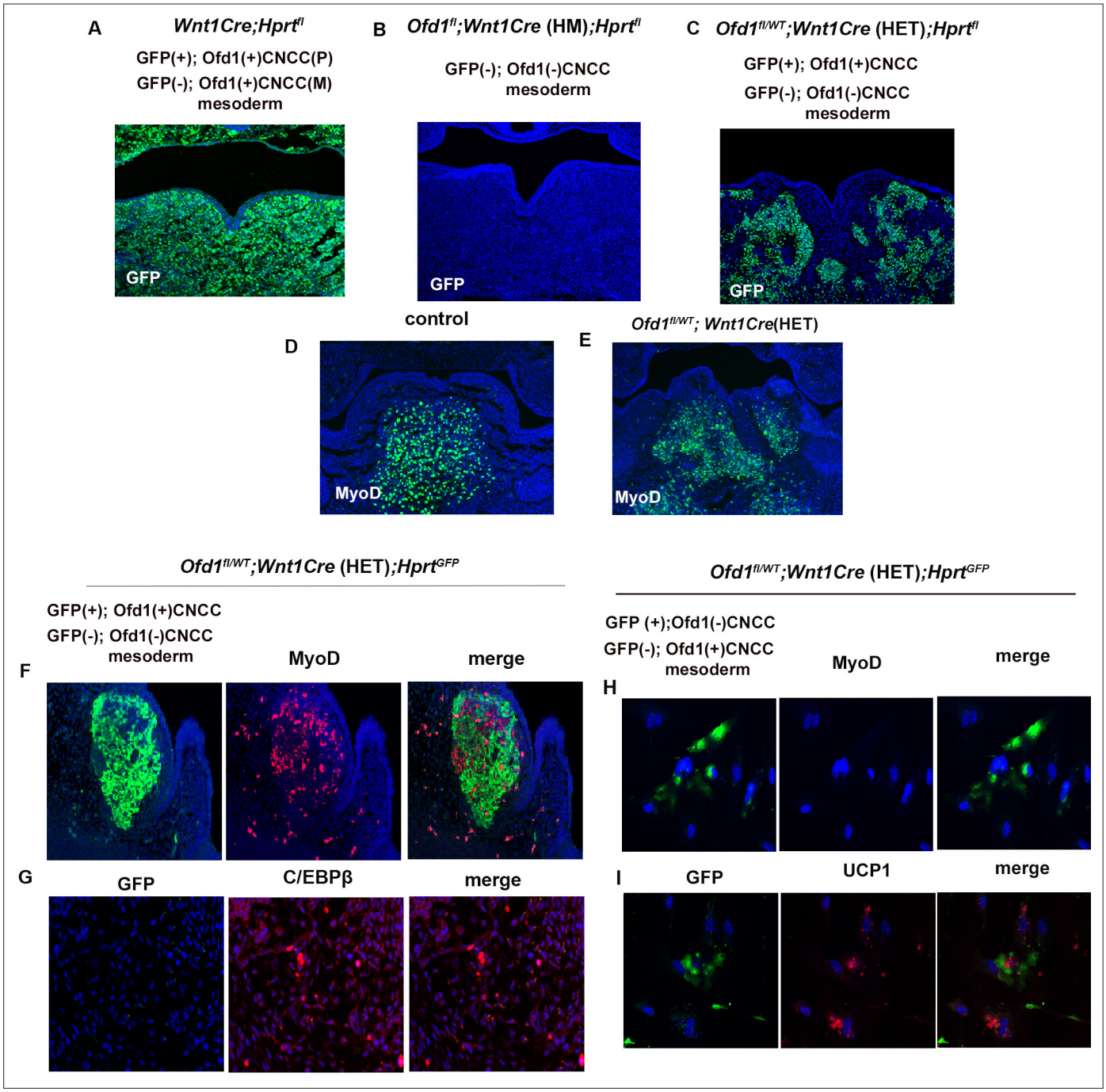

Figure 4. X-inactivation in *Ofd*1 mutant tongue. (**A–E**) Frontal sections showing immunohistochemistry of GFP (**A–C**) and MyoD (**D, E**) in *Wnt1Cre*(HET);*Hprt*^{fl} (**A**), *Ofd1*^{fl};*Wnt1Cre*(HM);*Hprt*^{fl} (**B**), *Ofd1*$^{fl/WT}$;*Wnt1Cre(HET);Hprt*^{fl} (**C**), wild-type (**D**), and *Ofd1*$^{fl/WT}$;*Wnt1Cre*(HET) (**E**) mice at embryonic day (E) 11. P, paternal; M, maternal. (**F, G**) Double immunohistochemistry of GFP and MyoD (**F**), and GFP and C/EBPβ (**G**) in *Ofd1*$^{fl/WT}$;*Wnt1Cre*(HET);*Hprt*^{fl} mice. (**H, I**) Double immunohistochemistry of GFP and MyoD (**H**), and GFP and UCP1 (**I**) on cultured YFP-expressing Ofd1 (-) cranial neural crest-derived cells (CNCC), GFP-negative mesoderm-derived cells, and GFP-negative Ofd1 (+) CNCC obtained from *Ofd1*$^{fl/WT}$;*Wnt1Cre*(HET);*Hprt*^{fl} mice.

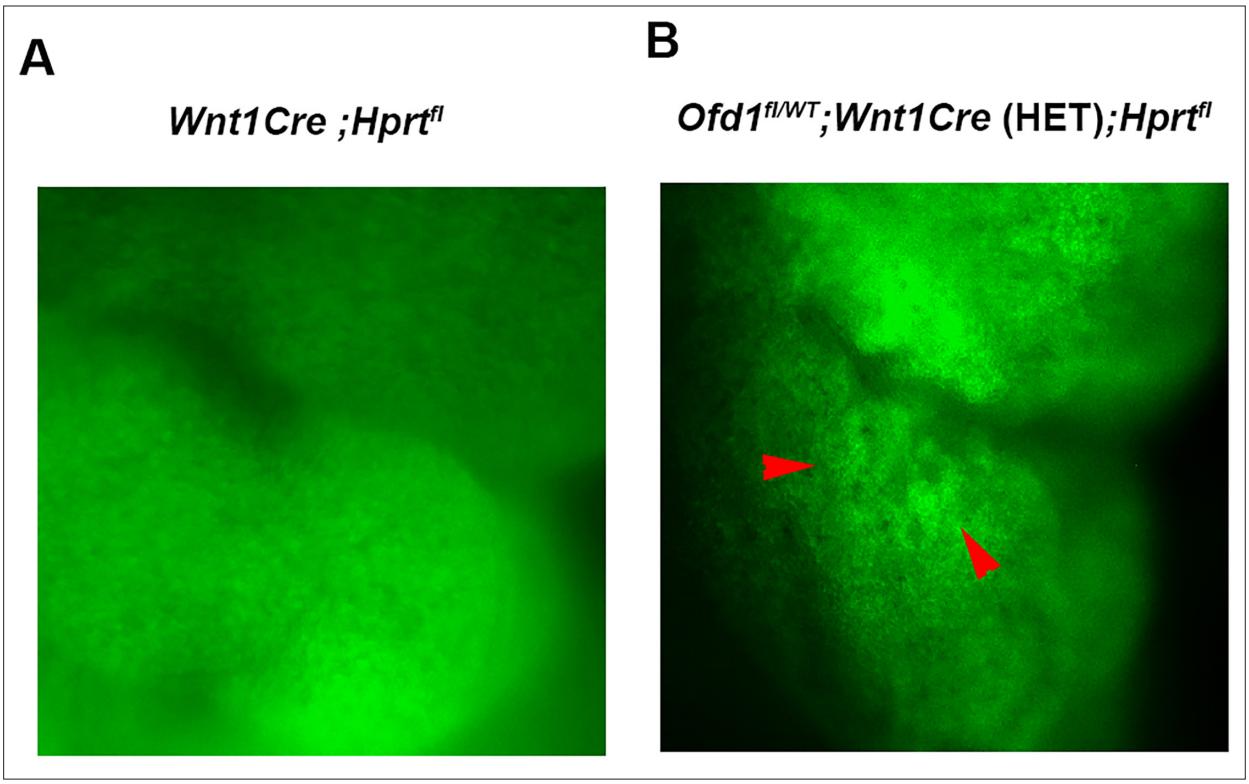

Figure 4—figure supplement 1. Cluster of *Ofd1* mutant cells in *Ofd1*$^{fl/WT}$;*Wnt1Cre*(HET) mice. Sagittal view of pharyngeal region of *Wnt1Cre;Hprt*^{fl} (**A**) and *Ofd1*^{fl};*Wnt1Cre*(HET);*Hprt*^{fl} (**B**). Arrowheads indicating cluster of GFP (-) cells.

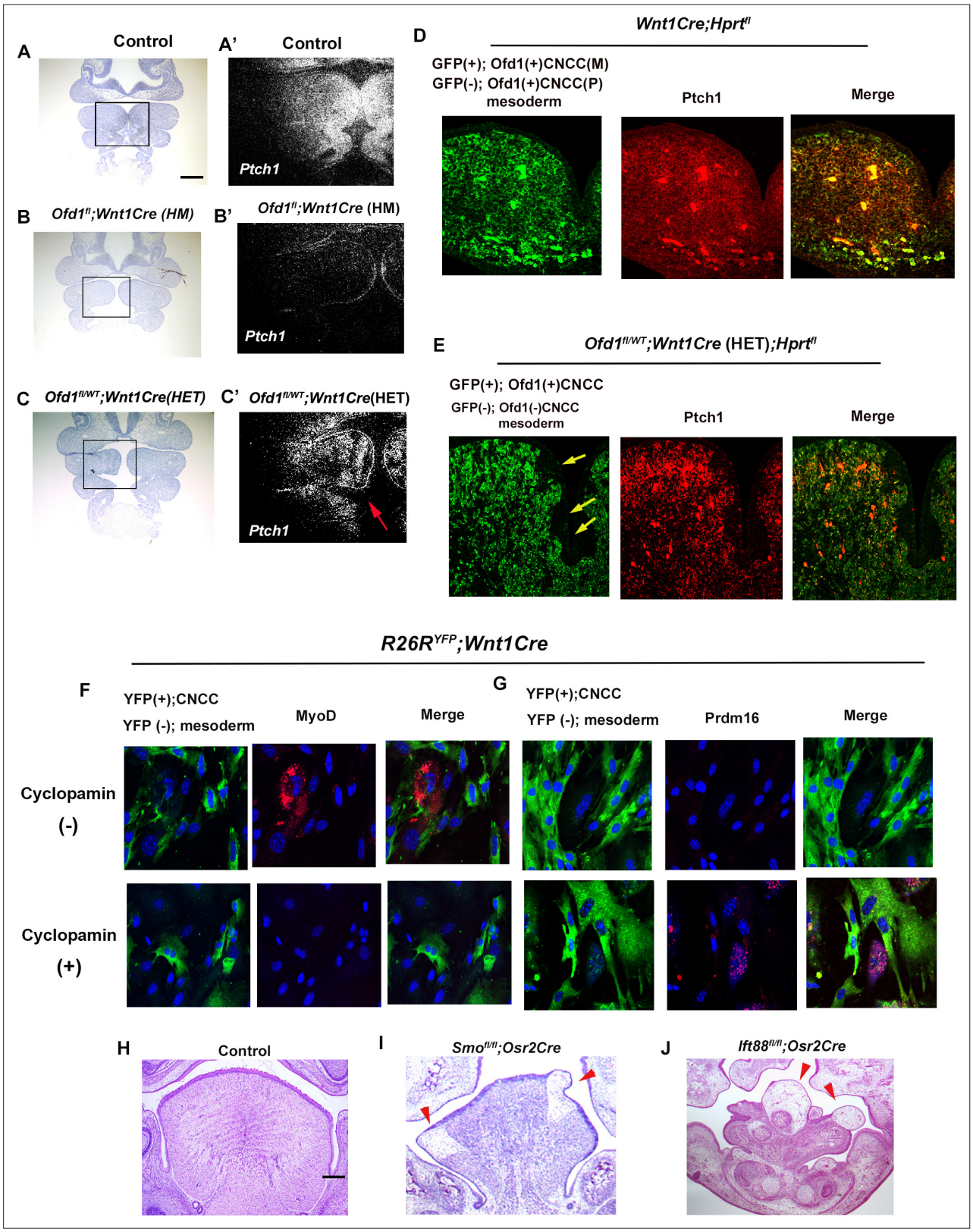

Figure 5. Hh signal in *Ofd1* mutant tongue. (**A–C'**) Frontal sections showing in situ hybridization of *Ptch1* in wild-type (**A'**), *Ofd1*^{fl};*Wnt1Cre*(HM) (**B'**), and *Ofd1*$^{fl/WT}$;*Wnt1Cre*(HET) (**C'**) at embryonic day (E) 10. A, B, C, bright field (counterstained section by hematoxylin) of A', B', C', respectively. A', B', C', high magnification of regions outlined by boxes in A, B, C, respectively. Arrow indicating mosaic *Ptch1* expression (**C'**). (**D, E**) Frontal sections showing double immunohistochemistry of GFP and Ptch1 in *Wnt1Cre;Hprt*^{fl} (**D**) and *Ofd1*$^{fl/WT}$;*Wnt1Cre*(HET);*Hprt*^{fl} (**E**) mice. Arrow indicating GFP-negative region (**E**). (**F,**

Figure 5 continued on next page

Figure 5 continued

G) Double immunohistochemistry of YFP and MyoD (**F**), and YFP and Prdm16 (**G**) on cultured YFP-expressing cranial neural crest-derived cells (CNCC) accompanied by YFP-negative mesoderm-derived cells obtained from *Wnt1Cre;R26R*^{YFP} mice with (lower panels) or without (upper panels) cyclopamine. (**H–J**) Frontal sections showing histology of wild-type (**F**), *Smo*$^{fl/fl}$*;Osr2Cre* (**G**), and *Ift88*$^{fl/fl}$*;Osr2Cre* (**H**) at E18.5. Arrowheads indicating ectopic sparse tissue. Scale bars: 100 μm (A-C'), 200 μm (H-J).

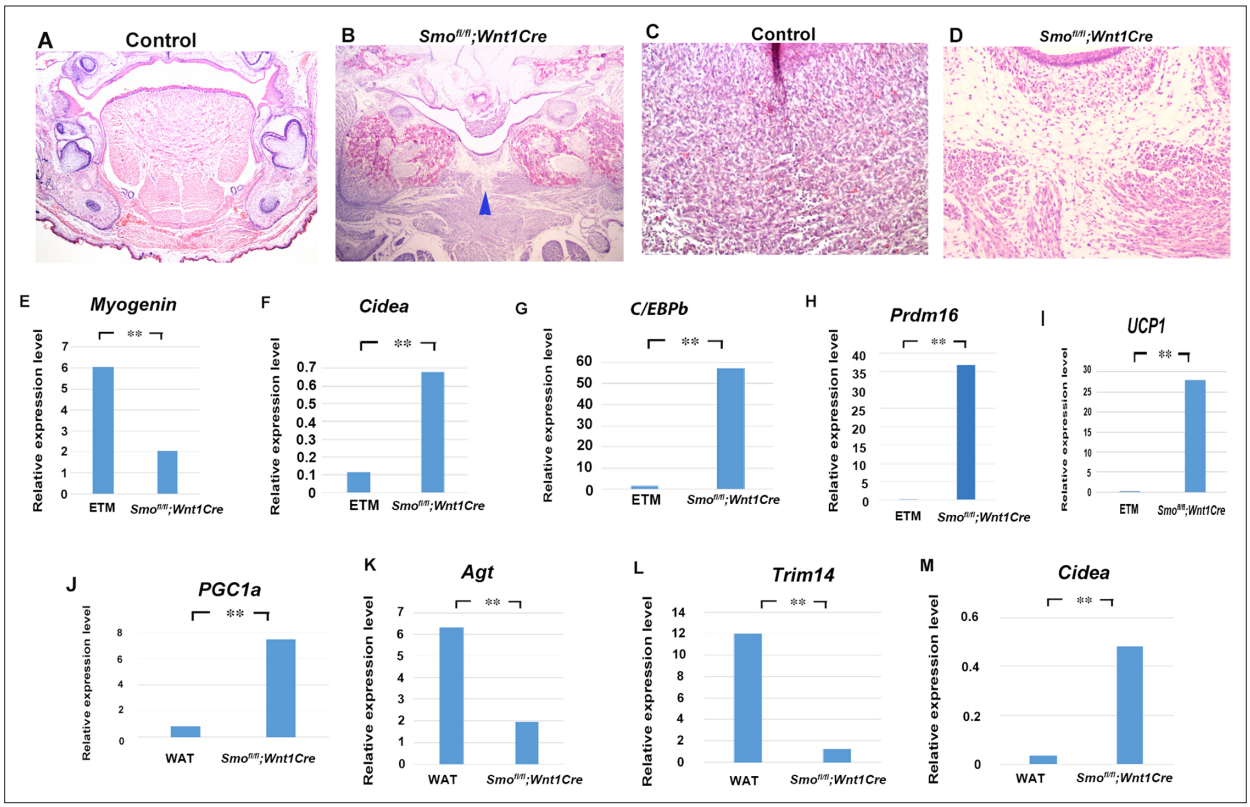

Figure 5—figure supplement 1. Adipose in *Smo* mutant mice. (**A–D**) Frontal section showing histological images of wild-type (**A, C**) and *Smo*$^{fl/fl}$*;Osr2Cre*(HM) (**B, D**) mice. B and D were high magnifications of A and C, respectively. (**E–M**) Quantitative PCR (q-PCR) on mRNA isolated from ectopic sparse tissue from *Smo*$^{fl/fl}$*;Wnt1Cre*, embryonic tongue muscle (ETM), and white adipose tissue (WAT). **p<0.01.

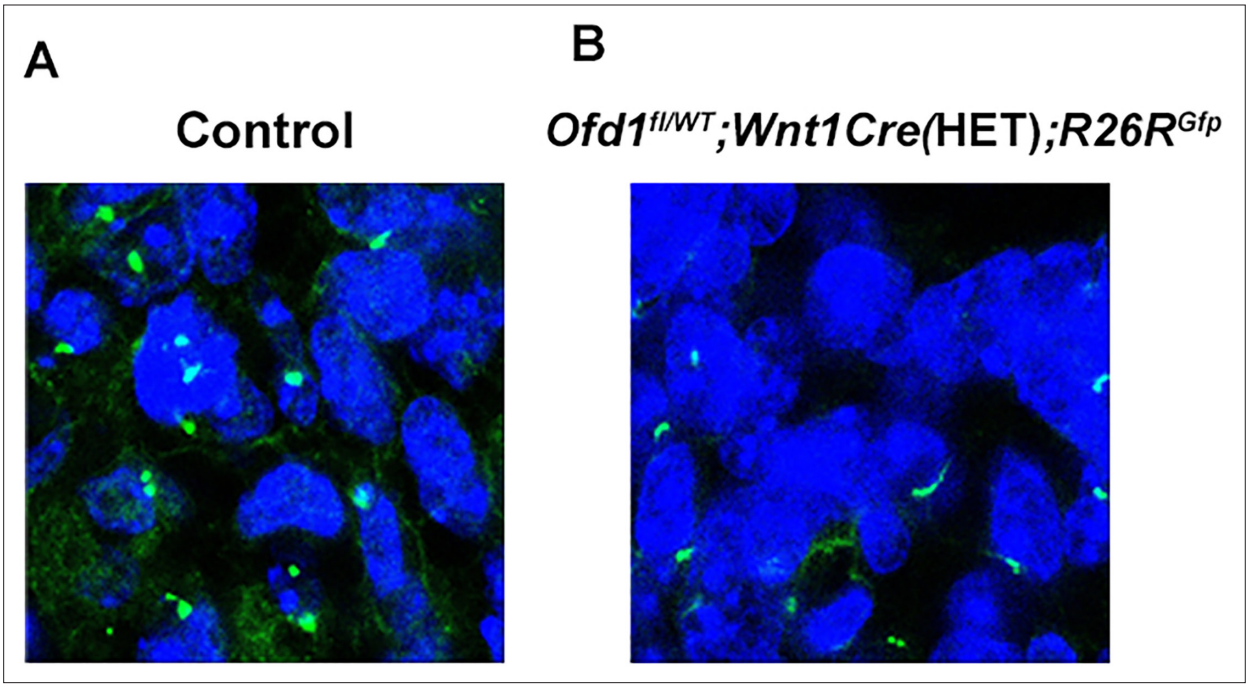

Figure 5—figure supplement 2. Acetylated α-tubulin in cranial neural crest-derived cells (CNCC) during tongue development. Frontal section showing immunohistochemistry of acetylated α-tubulin in YFP-expressing cells of *Wnt1Cre*(HET);*R26R*^{Yfp} (**A**) and *Ofd1*$^{fl/WT}$;*Wnt1Cre*(HET);*R26R*^{Yfp} mice (**B**). CNCC were confirmed by YFP expression.

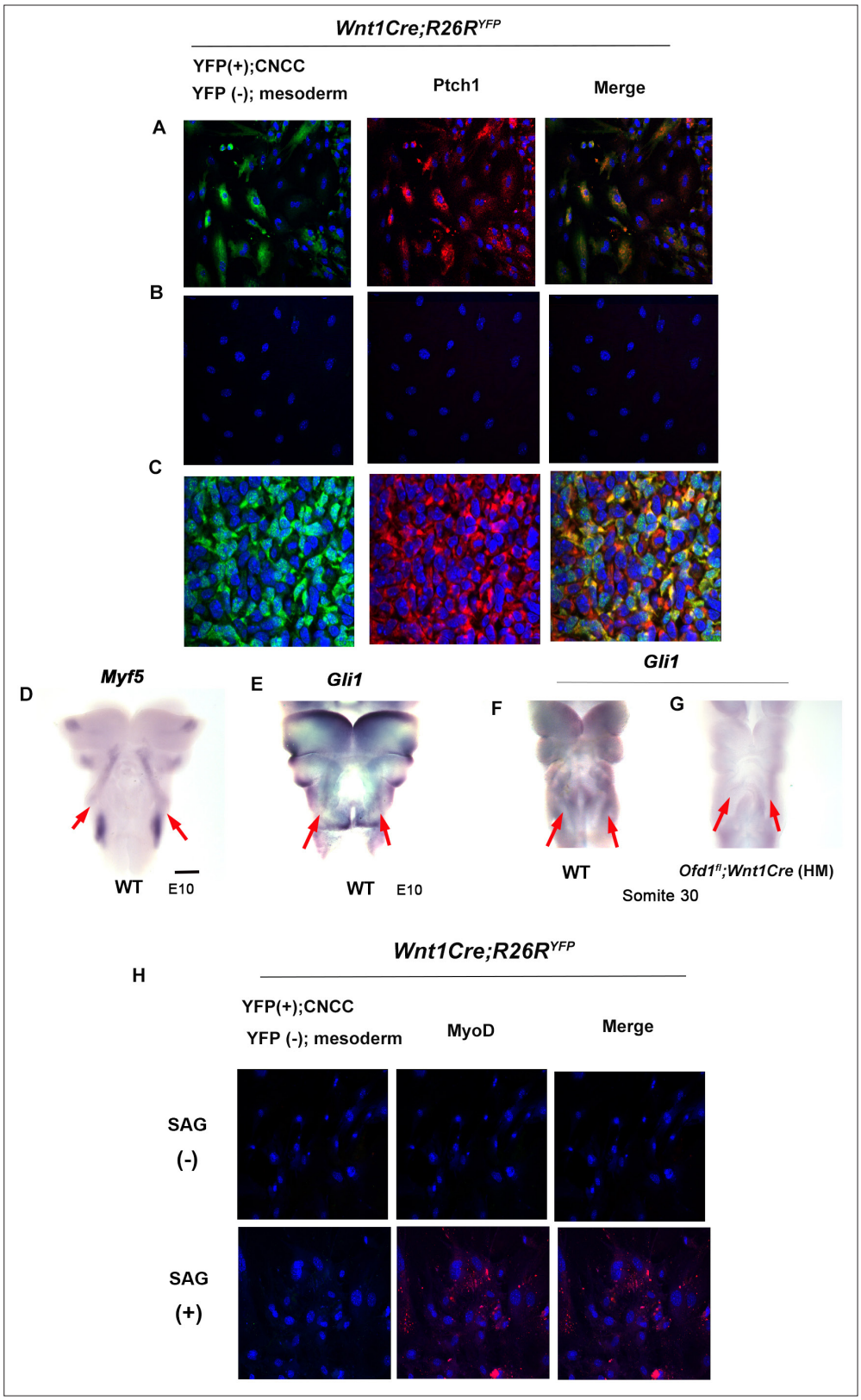

Figure 6. Hh signal in mesoderm-derived cells. (**A, B**) Double immunohistochemistry of YFP and Ptch1 on cultured YFP-expressing cranial neural crest-derived cells (CNCC) accompanied by YFP-negative mesoderm-derived cells (**A**) and only YFP-negative mesoderm-derived cells (**B**) obtained from *Wnt1Cre;R26R*^{YFP} mice. (**C**) Double immunohistochemistry of YFP and Ptch1 in *Wnt1Cre;R26R*^{YFP} mice. (**D–G**) Frontal images of whole-mount in situ

Figure 6 continued on next page

Figure 6 continued

hybridization of *Myf5* (**D**) and *Gli1* (**E–G**) in wild-type (**D–F**) and *Ofd1*^{fl};*Wnt1Cre*(HM) (**G**) at embryonic day (E) 10. (**H**) Double immunohistochemistry of YFP and MyoD on cultured YFP-negative mesoderm-derived cells obtained from *Wnt1Cre;R26R*^{YFP} mice with (lower panels) or without (upper panels) SAG. Scale bars: 500 μm (D-G).

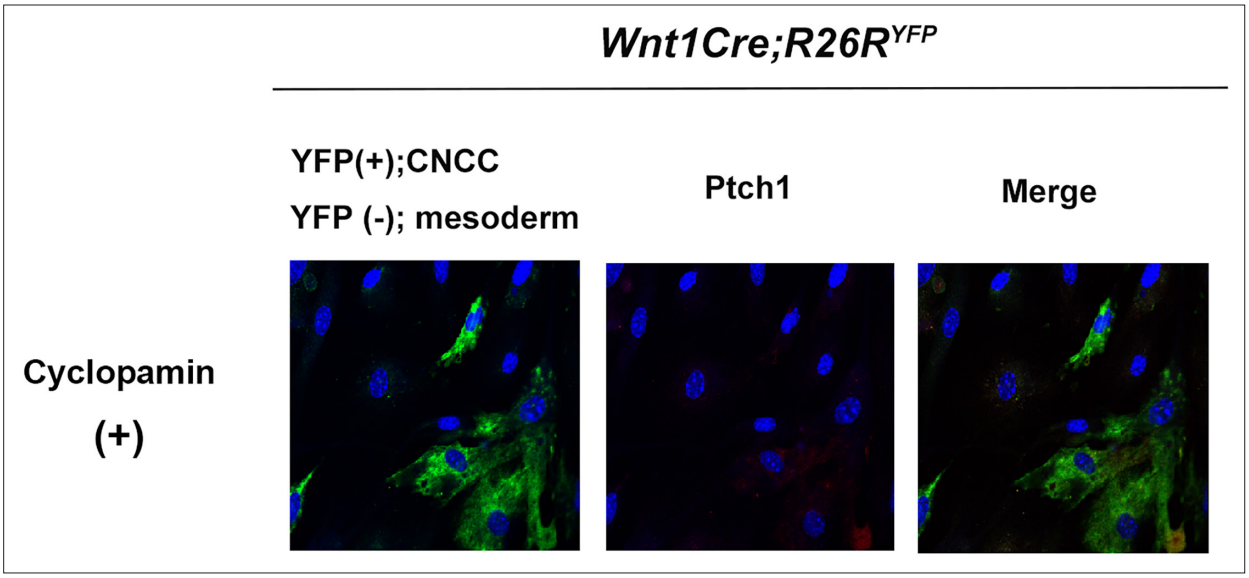

Figure 6—figure supplement 1. Cyclopamine treated cranial neural crest-derived cells (CNCC) and mesoderm-derived cells. Double immunohistochemistry of YFP and Ptch1 on cultured YFP-expressing CNCC accompanied by YFP-negative mesoderm-derived cells obtained from *Wnt1Cre;R26R*^{YFP} mice with cyclopamine.

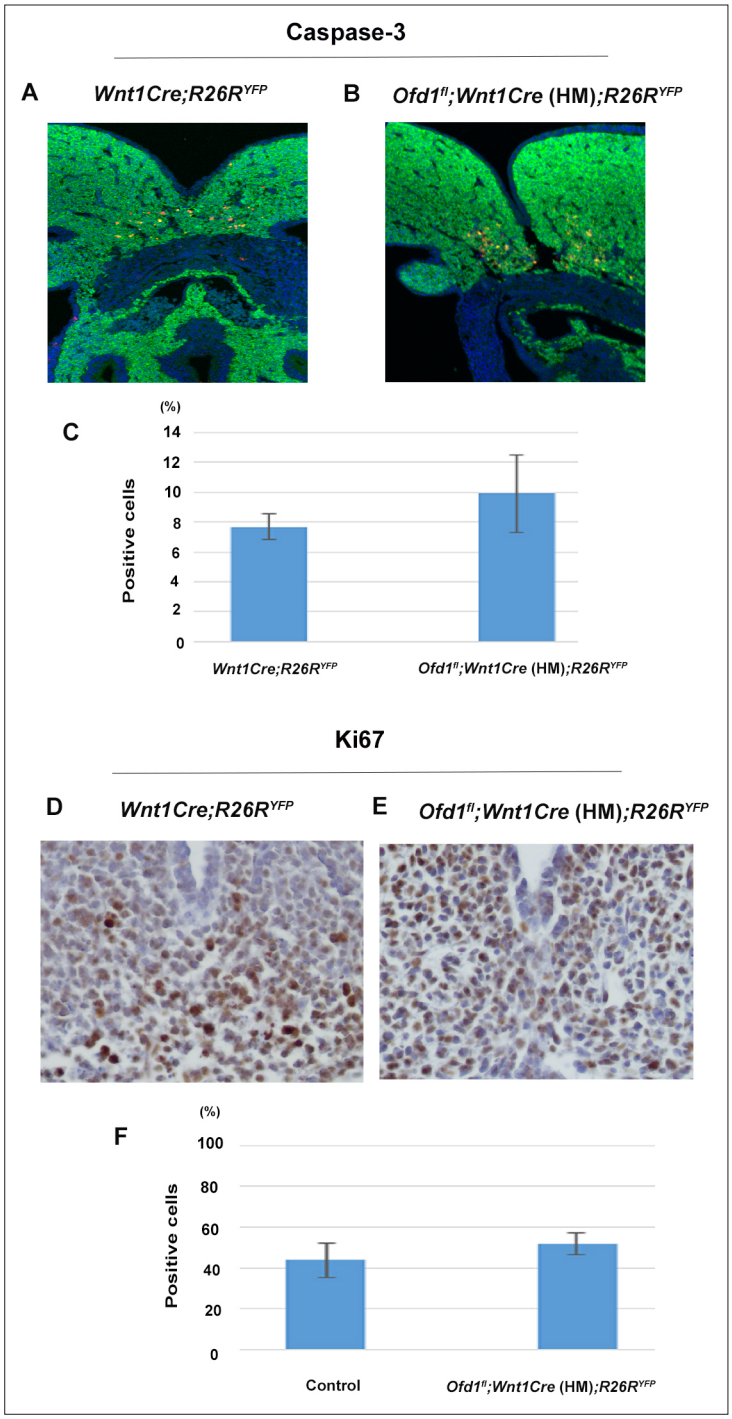

Figure 6—figure supplement 2. Apoptosis and cell proliferation in *Ofd1* mutant tongue. (**A, B**) Frontal sections showing Caspase-3 immunohistochemistry. (**C**) Comparison of the number of Caspase-3-positive cells between *Wnt1Cre;R26R*^{YFP} mice and *Ofd1*^{fl}*;Wnt1Cre*(HM)*;R26R*^{YFP} mice. (**D, E**) Frontal sections showing Ki67-positive cells. (**F**) Comparison of the number of Ki67-positive cells between *Wnt1Cre;R26R*^{YFP} mice and *Ofd1*^{fl}*;Wnt1Cre*(HM)*;R26R*^{YFP} mice.

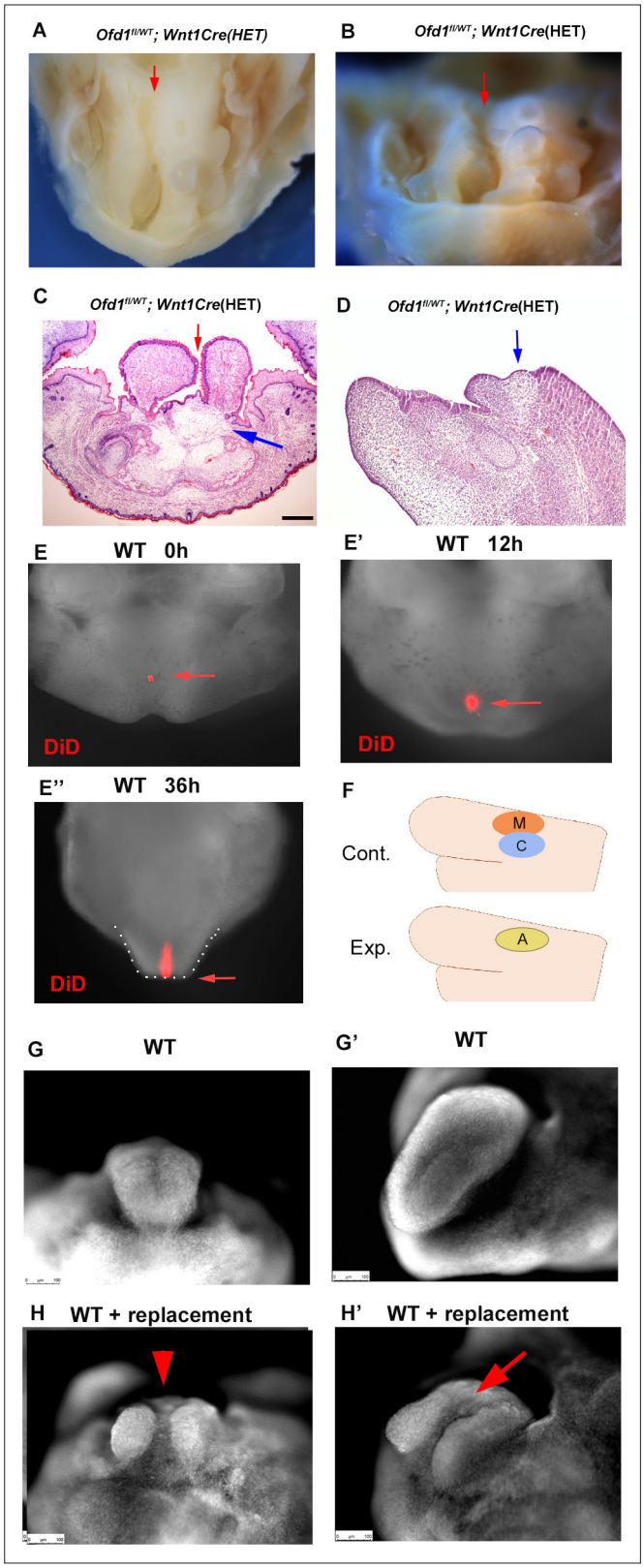

Figure 7. Clefts in *Ofd1* mutants. (**A, B**) Oral (**M**) and frontal (**N**) view of *Ofd1*$^{fl/WT}$;*Wnt1Cre*(HET) mice. Arrows indicating cleft. (**C, D**) Frontal (**C**) and sagittal (**D**) sections showing histological images. Blue and red arrows indicating sparse tissue and cleft, respectively. (**E–E''**) Nuclear fluorescent image showing oral view of wild-type mandible with DiD at embryonic day (E) 11.5 before culture (**E**), 12 hr (**E'**), and 36 hr (**E''**) after culture. Arrow

Figure 7 continued on next page

Figure 7 continued

indicating DiD labeled cells. Tongue-like structure is outlined by white dots (**E″**). (**F**) Schematic diagram showing sagittal view of mandible exhibiting replacement of cranial neural crest-derived cells (CNCC) (C, blue circle) and myoblasts (M, red circle) into adipose tissue (A, yellow circle). (**G–H′**) Nuclear fluorescent image showing frontal (**G, H**) and oral (**G′, H′**) view of wild-type mandible without (**G, G′**) and with (**H, H′**) replacement. Scale bars: 200 μm (C, D).

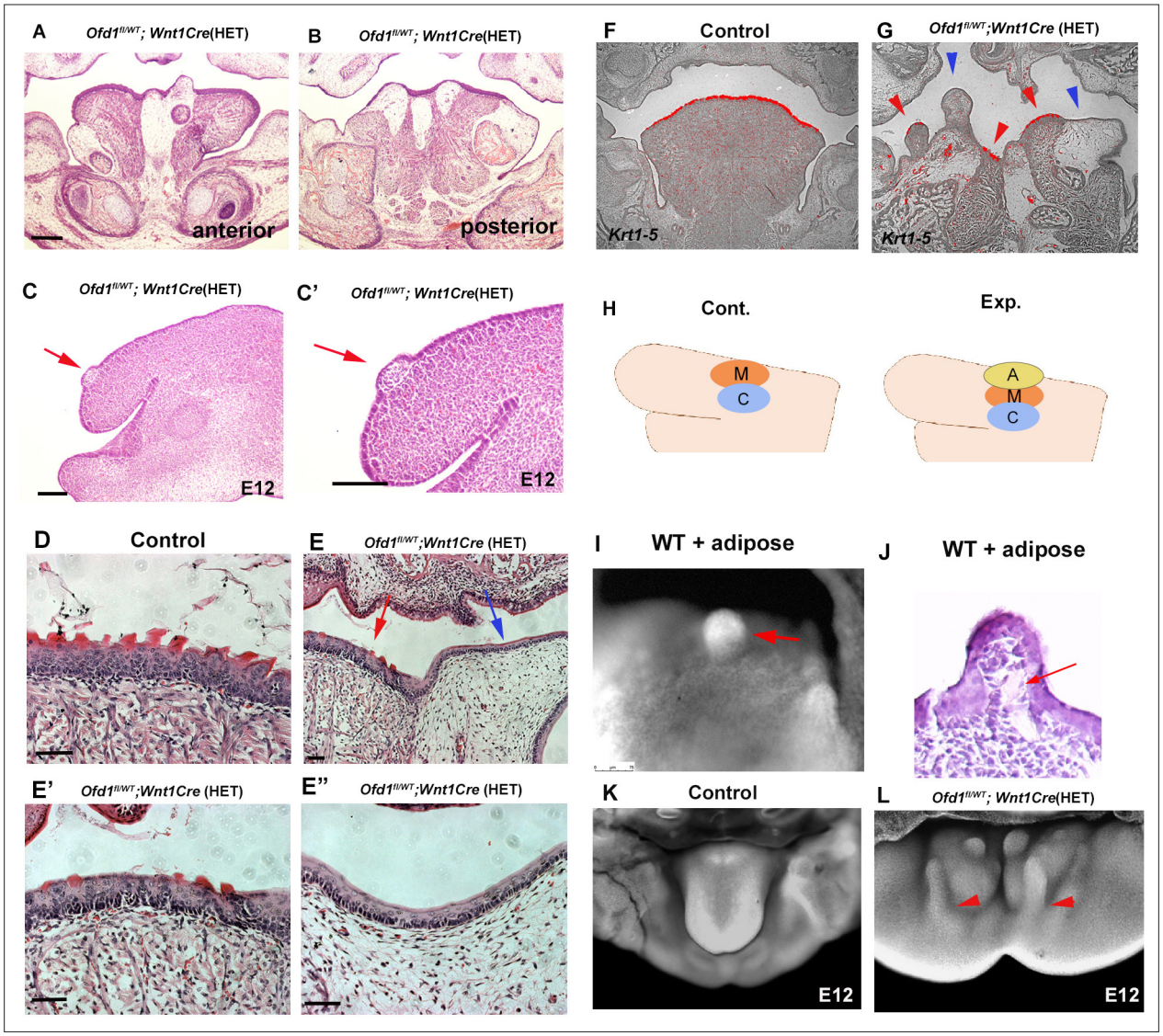

Figure 8. Adipose tissue in *Ofd1* mutant tongue. (**A, B, C–E″**) Frontal (**A, B, D–E″**) and sagittal (**C, C′**) sections showing histological images in wild-type (**D**), and *Ofd1*$^{fl/WT}$;*Wnt1Cre*(HET) (**A–C′, E–E″**). E′ and E″ are high magnification of E. (**F, G**) Frontal sections showing in situ hybridization of *Krt1-5* in wild-type (**F**) and *Ofd1*$^{fl/WT}$;*Wnt1Cre*(HET) (**G**). (**H**) Schematic diagram showing sagittal view of mandible exhibiting graft of adipose tissue (A, yellow circle), cranial neural crest-derived cells (CNCC) (C, blue circle) and myoblasts (M, red circle). (**I**) Nuclear fluorescent image showing dorsum of tongue in cultured mandible with grafting. (**J**) Histological images of dorsum of tongue in cultured mandible with grafting. (**K, L**) Nuclear fluorescent image showing oral view of developing mandibles in wild-type (**K**) and *Ofd1*$^{fl/WT}$;*Wnt1Cre*(HET) (**L**). Arrowheads indicating protrusion into the floor of mandible from the dorsum surface of tongue swelling (**L**). Scale bars: 200 μm (A, B, F, G), 100 μm (C-E″).

Figure 9. Tongue in OFD1 patient. (**A, B**) Tongue in OFD1 patient (G138S missense mutation). Arrowheads and arrows indicating protruded tissue and normal tongue, respectively. (**C–L, O–R**) Sections showing histological images (**C–H, O, P**) and immunohistochemistry of Prdm16 (**I, J**), UCP1 (**K, L**), and KRT1-5 (**Q, R**) on control human tongue (**C, D, O, Q**) and OFD1 patient tongue (**E–H, J, L, P, R**). (**M, N**) Quantitative PCR (q-PCR) on mRNA isolated from ectopic sparse tissue from OFD1 patient tongue, cultured human skeletal muscle myoblasts (CHM), and cultured human white adipocyte (CHWA).

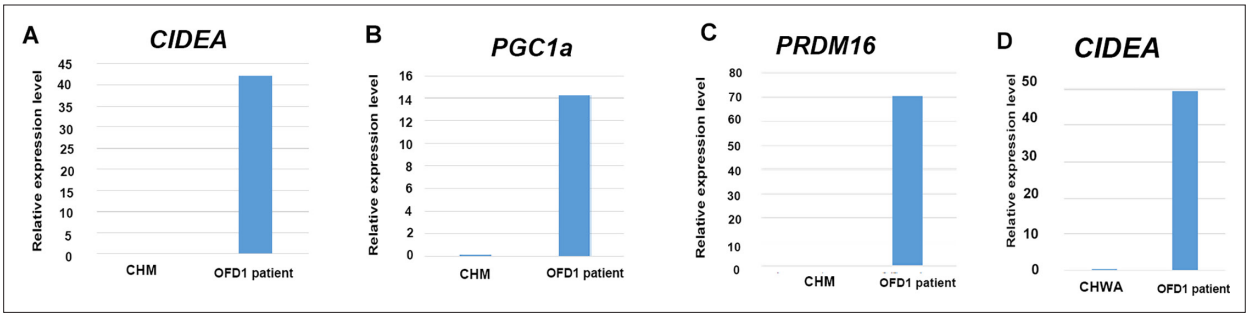

Figure 9—figure supplement 1. Quantitative PCR (q-PCR) analysis on OFD1 patient tongue. q-PCR of CIDEA (**A**), PGC1a (**B**), PRDM16 (**C**) and CIDEA (**D**) on mRNA isolated from ectopic sparse tissue from OFD1 patient tongue, cultured human myoblasts (CHM), and cultured human white adipocytes (CHWA).

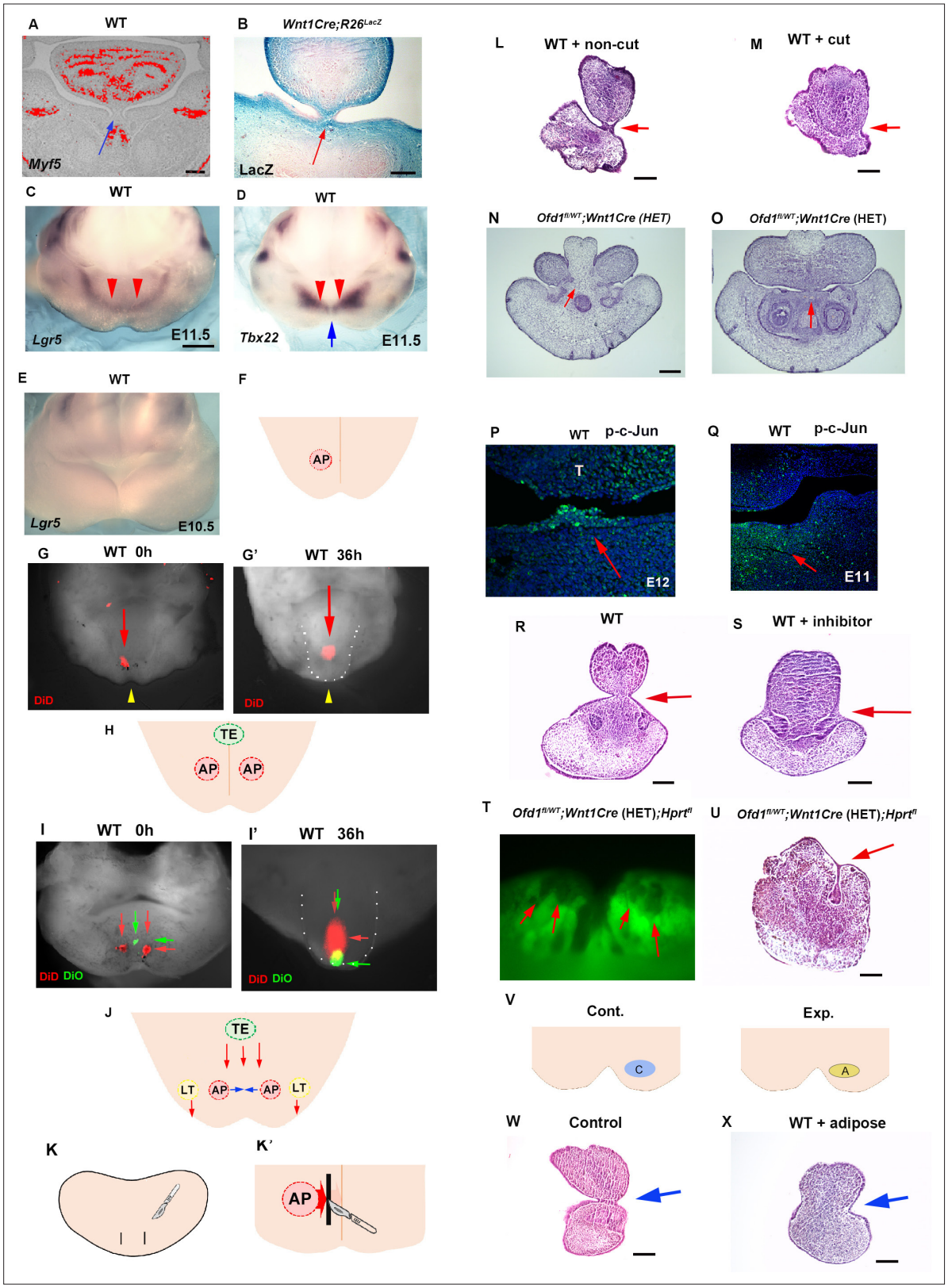

Figure 10. Tongue frenum in *Ofd1* mutant mice. (**A, B**) Frontal sections showing in situ hybridization of *Myf5* (**A**) and LacZ staining (**B**) in wild-type (**A**) and *WntCre;R26R*^{LacZ} (**B**). Arrows indicating tongue frenum region. (**C–E**) Oral view of whole-mount in situ hybridization of *Lgr5* (**C, E**) and *Tbx22* (**D**) in wild-type at embryonic day (E) 11.5 (**C, D**) and E10.5 (**E**). Red and blue arrows indicating anterior expression domain and midline region, respectively. (**F, H**) Schematic diagram showing oral view of mandible with AP (light red) and TE region (light green), and midline (orange line). (**G, G', I, I'**) Nuclear

Figure 10 continued on next page

Figure 10 continued

fluorescent image showing oral view of wild-type mandible before (**G, I**) and after (**G′, I′**) culture. Red and green arrows indicating DiD and DiO, respectively. Yellow arrowheads indicating midline. (**G′, I′**) Tongue-like structure was partially removed and presumptive tongue-like structure are outlined by white dots. (**J**) Schematic diagram showing oral view of mandible with movement of cells in AP (light red), LT (light yellow), and TE region (light green line). (**K, K′**) Schematic diagram showing oral view of mandible with incision (black line) and midline (orange line). (**L, M**) Frontal sections showing histological images of cultured jaw without incision (**L**) and with incision (**M**). Arrows indicating the tongue frenum region. Tongue frenum formation with, n=1/6 and without incision, n=8/10. (**N, O**) Frontal sections showing histological images in *Ofd1*$^{fl/WT}$;*Wnt1Cre*(HET) mice obtained from same mouse (O; more posterior site than N). (**P, Q**) Frontal sections showing immunohistochemistry of p-c-Jun in wild-type at E12 (**P**) and E11 (**Q**). Arrows indicating positive cells in the tongue frenum (**P**) and AP region (**Q**). (**R, S**) Frontal sections showing histological images of cultured jaw with (**S**) and without U73122 (**R**). Arrows indicating the tongue frenum region. Tongue frenum formation with U73122, n=0/4. (**T**) Oral view of mandible in *Ofd1*$^{fl/WT}$;*Wnt1Cre*(HET);*Hprt*^{fl} mice. Arrows indicating Gfp-negative domains around AP region before culture. (**U**) Frontal sections showing histological images of T after culture. Arrow indicating tongue frenum region. (**V**) Schematic diagram showing oral view of mandible with replacement (A, yellow circle=adipose, blue circle=cranial neural crest-derived cell [CNCC]). (**W, X**) Frontal sections showing histological images of cultured jaw without replacement (**W**) and with replacement (**X**). Arrows indicating tongue frenum region. Tongue frenum formation with replacement, n=1/5. Scale bars: 200 μm (A, B, L, M, N, O, R, S, U, W, X), 500 μm (C-E).

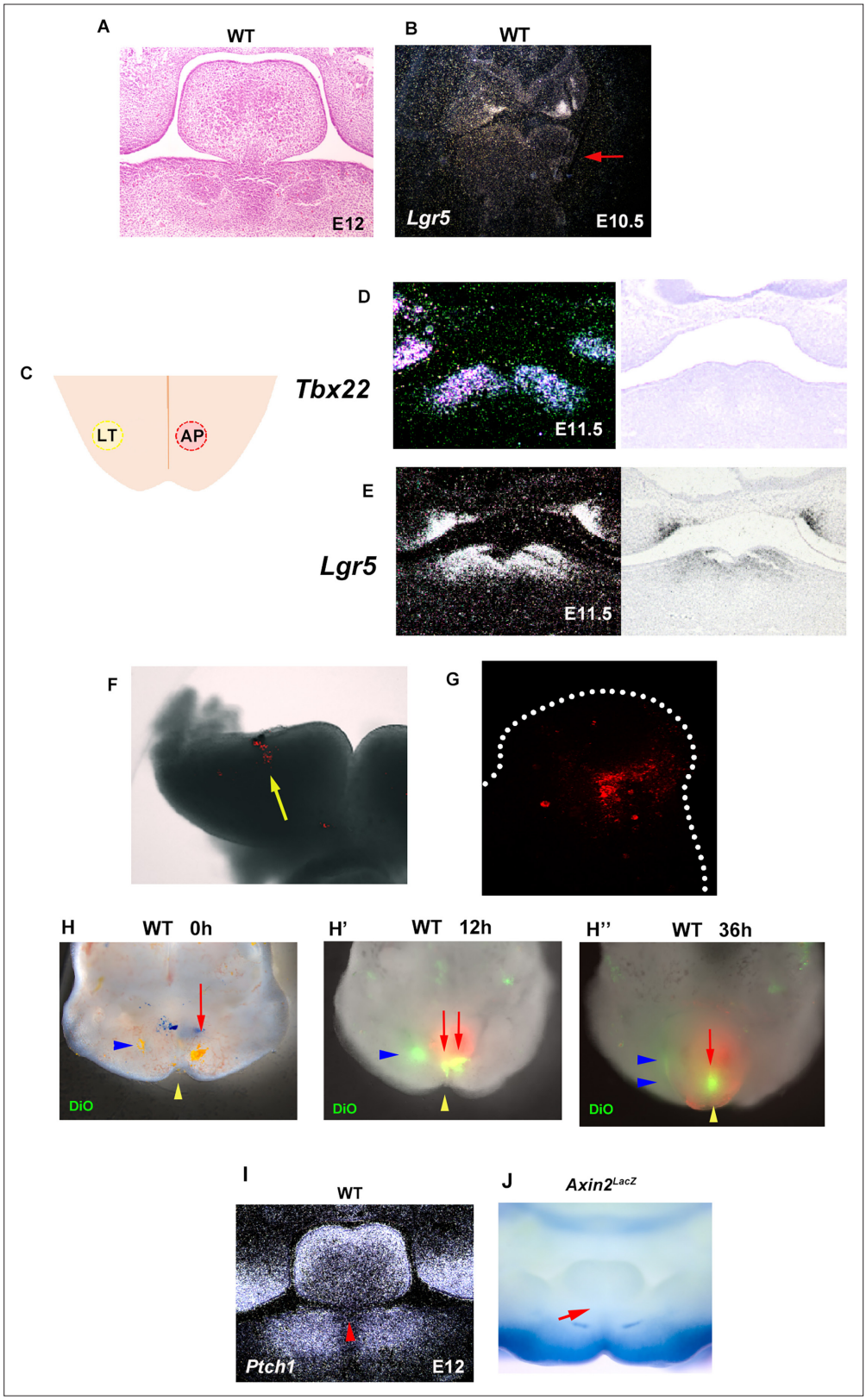

Figure 10—figure supplement 1. Tongue frenum formation in wild-type mice. (**A, B**) Frontal section showing histological image (**A**) and in situ hybridization of *Lgr5* (**B**) of tongue frenum (**A**) and mandible (**B**) in wild-type mice at embryonic day (E) 10.5 (**B**) and E12.5 (**A**). Arrow indicating mandible region. (**C**) Schematic diagram showing oral view of mandible with LT (yellow ceircle) and AP (right red circle) region, and midline (orange line). (**D, E**) Frontal

Figure 10—figure supplement 1 continued on next page

Figure 10—figure supplement 1 continued

sections showing in situ hybridization of *Tbx22* (**D**) and *Lgr5* (**E**) at E11.5. Left panels, dark field; right panels, bright fields. (**F**) Frontal image showing mandibular process with DID injection before culture. Arrow indicating DID. (**G**) Sagittal section showing mandible with DID after culture. Tongue was outlined by white dots. (**H–H″**) Oral view of wild-type mandible with DiO injection (H, 0 hr, H′, 12 hr, H″, 36 hr after injection). Blue arrowheads and red arrows indicating DiO at LT and AP region, respectively. Yellow arrowhead indicating midline. (**I**) Frontal sections showing in situ hybridization of *Ptch1* at E12.5. (**J**) Frontal view of mandible in LacZ stained *Axin2*^{LacZ} mice at E12.5. Arrows and arrowhead indicating tongue frenum region (**E, F**).